



JGR Atmospheres

L

RESEARCH ARTICLE

10.1029/2025JD044488

Key Points:

- Intertwined microphysical and multiscale dynamical processes shape contrail lifetime statistics in three distinct evolutionary regimes
- Mesoscale temperature fluctuations induced by high frequency gravity waves cause a wide range of contrail lifetimes
- Deep ice-supersaturated layers, large turbulent diffusivity, and ice nucleation at contrail tops may increase maximum contrail lifetimes

Correspondence to:

B. Kärcher, bernd.kaercher@dlr.de

Citation:

Kärcher, B., & Corcos, M. (2025). On the lifetimes of persistent contrails and contrail cirrus. *Journal of Geophysical Research: Atmospheres*, *130*, e2025JD044488. https://doi.org/10.1029/2025JD044488

Received 1 JUN 2025 Accepted 9 OCT 2025

Author Contributions:

Conceptualization: Bernd Kärcher,

Investigation: Bernd Kärcher,

Milena Corcos

Methodology: Bernd Kärcher, Milena Corcos

Writing – original draft: Bernd Kärcher Writing – review & editing:

Bernd Kärcher, Milena Corcos

On the Lifetimes of Persistent Contrails and Contrail Cirrus

Bernd Kärcher¹ and Milena Corcos²

¹Institut für Physik der Atmosphäre, DLR Oberpfaffenhofen, Wessling, Germany, ²NorthWest Research Associates, Boulder, CO, USA

Abstract Prediction of contrail cirrus persistence is highly problematic for models, in part due to a poor representation of intertwined microphysical and dynamical processes controlling contrail evolution in largescale ice-supersaturated areas. Knowledge of contrail cirrus lifetimes is required to estimate their lifecycleaverage radiative effect, but lifetime statistics inferred from observations are incomplete, hampering model validation. Contrail cirrus ice crystal size distributions are mainly impacted by entrainment and plume dilution, ice deposition growth and sublimation, and gravitational settling. Changes in the size distributions are due to synoptic and mesoscale air motions that affect sign and magnitude of ice supersaturation experienced by contrail particles. Driven by internal gravity waves, rapid growth/sublimation cycles and sedimentation lead to a selection of ice crystal sizes enabling long lifetimes for persistent contrails whose evolution is not limited by synoptic warming. Wave-induced mesoscale supersaturation fluctuations lead to a wide spectrum of lifetimes with mean values of 24 hr and maxima up to 16 hr in large-scale ice-saturated conditions. Even longer maximum lifetimes as seen in some observations are possible within deep ice-supersaturated layers, enhanced microscale turbulent temperature fluctuations, and new ice formation at the top of contrail cirrus. We conceptualize lifetime statistics and define initial adjustment, intermediate stabilization, and final dissipation regimes. Our analysis of contrail cirrus lifetimes and ice crystal size distributions will aid future satellite analyses and model development.

Plain Language Summary The climate impact of aviation should be reduced due to its increasing contribution to global warming. Although the climate effect of aviation carbon dioxide emissions is well understood, the role of contrails and the cirrus clouds evolving from them is much less clear. Models used to explore the effectiveness of contrail mitigation options are highly simplified and need to be benchmarked against more detailed scientific research models. At the same time, important information to be used to inform and constrain contrail models is lacking. Here we investigate factors controlling contrail lifetimes based on state-of-the-art, physics-based descriptions of the underlying processes. The keystone of the present study is the systematic investigation of how lifetime statistics depend on both vertical air motions from weather scales to the scale of individual contrails, ice microphysical processes operating within contrails, and their interaction. The insights and results presented here might help advance contrail models and parameterizations employed in climate models, with the goal to better predict the climate impact of aviation-induced cloudiness.

1. Introduction

Reaching and sustaining net zero global anthropogenic carbon dioxide (CO_2) emissions and declining net non- CO_2 impacts would halt anthropogenic global warming on multi-decadal timescales (Forster et al., 2021). Aviation impacts Earth's climate through emissions of long-lived CO_2 and transient non- CO_2 effects that are unique to this sector of transportation (Fahey & Schumann, 1999). Under a sustained pre-pandemic air traffic growth path, global aviation contributes up to 17% of the global warming budget left in 2050 to stay within the $1.5\,^{\circ}$ C limit (Klöwer et al., 2021). Achieving net zero aviation CO_2 emissions—by itself already a tall order—without at the same time reducing its non- CO_2 impacts may compromise the alignment of the aviation sector with the goal of the 2015 Paris agreement (Brazzola et al., 2022; Grewe et al., 2021).

Long-lived (persistent) contrails may form contrail clusters and transform into cirrus-like clouds—together denoted as aircraft-induced cloudiness (AIC)—that may eventually no longer be separated from natural cirrus. AIC contributes significantly to the total aviation non- CO_2 impact (Kärcher, 2018). Together, emissions of CO_2 and the formation of AIC give rise to the majority of the radiative forcing (RF) from aviation (Lee et al., 2021). Reducing the net warming due to AIC co-benefits reductions in aviation CO_2 emissions. However, assessing the relative importance of aviation CO_2 emissions and AIC to global warming is challenging (Borella et al., 2024).

© 2025. The Author(s). This is an open access article under the terms of the Creative Commons Attribution License, which permits use, distribution and reproduction in any medium, provided the original work is properly cited.

KÄRCHER AND CORCOS 1 of 28

RF arising from aircraft-emitted CO_2 and the associated long-term, global mean near-surface temperature change can be quantified with a reasonable level of confidence, as estimates of the CO_2 climate sensitivity relating both parameters can be applied (Ramaswamy et al., 2019). By contrast, quantifying the respective climate impact parameters of AIC is associated with a much higher level of scientific uncertainty (Lee et al., 2023). The few model studies addressing this issue (Bickel et al., 2020, 2025; Ponater et al., 2005; Rap et al., 2010) suggest a potentially low efficacy of contrail cirrus to force global warming.

Persistent contrails and contrail cirrus form in cold and sufficiently moist upper tropospheric air, are advected with air parcels through weather systems, and are affected by the same processes as natural cirrus (Burkhardt & Kärcher, 2009). A crucial factor impacting AIC evolution is ice supersaturation, s, defined as the fractional relative humidity relative to ice saturation. Supersaturation is affected by moisture transport and vertical air motion down to the smallest atmospheric scales (Kärcher et al., 2024). Large AIC RF occurs in large-scale ice-supersaturated areas in regions with dense air traffic (Burkhardt et al., 2018). Current global models struggle to reproduce the observed magnitude and spatio-temporal variability in vertical wind speeds, hence temperature and s, at the mesoscale (Köhler et al., 2023; Podglajen et al., 2020; Polichtchouk et al., 2021), which includes the scale of individual contrails or contrail clusters.

AIC is a short-lived climate forcer, potentially making it amenable for swift mitigation. Mitigating the climate impact of AIC is scientifically challenging and technologically complex (Lee et al., 2023) and likely requires a combination of options (Kärcher, 2018). In view of the limited environmental efficiency of carbon offsetting, associated atmospheric and technological tradeoffs demand careful consideration (Becken & Mackey, 2017).

A strategy that aims to avoid persistent contrail formation via flight route diversions on a flight-by-flight basis (navigational avoidance) has been suggested as an immediate option to mitigate the AIC impact (Teoh et al., 2020). The application of such a strategy would require, among other things, accurate forecasts of time, duration, location, spatial extent, and physical properties of ice-supersaturated areas and cirrus clouds down to the scale of individual flight path segments. However, upper tropospheric ice supersaturation and cirrus properties are not conventionally analyzed in global atmospheric models. Predicting individual contrail persistence based on a state-of-the-art numerical weather model is problematic due to poorly simulated ice supersaturation (Gierens et al., 2020). Gravity waves, mostly unresolved in global models, determine to a large extent the frequency of occurrence of ice-supersaturated states at the cloud scale (Kärcher et al., 2023). Thus, any implementation of AIC formation and evolution should be carefully documented and validated.

As global weather and climate models move to higher resolution, improving the representation of small-scale dynamical and microphysical processes affecting cirrus clouds, and thus AIC, becomes a priority. These processes include mesoscale temperature fluctuations due to gravity waves (Podglajen et al., 2016) and kinetic limitations of water vapor uptake during diffusional cloud ice crystal growth and sublimation (C. Zhang & Harrington, 2014). They are important for describing natural cirrus, but are only poorly, if at all, represented in atmospheric models. Therefore, global and plume-scale models (Bock & Burkhardt, 2016; Caiazzo et al., 2017; Chen & Gettelman, 2013; Fritz et al., 2020; Schumann, 2012; W. Zhang et al., 2025) and their underlying parameterizations used to predict AIC need to properly account for these effects as well.

Contrails and contrail cirrus interact with solar and terrestrial radiation (Wolf et al., 2023). Cloud-radiation interactions become potentially more relevant as cloud lifetimes increase, thus AIC lifetimes must be known to calculate the associated lifecycle-integrated RF (Burkhardt & Kärcher, 2011). The potentially large radiative impact of AIC is desirable to avoid. Knowledge of AIC lifetimes is thus also relevant for mitigation (Gryspeerdt et al., 2024). To this date, however, this topic has received only little attention. Recently, a model study presented a timescale analysis of lifetime constraints due to synoptic motion and cloud ice sedimentation (Hofer & Gierens, 2025). Here we go an important step further by including mesoscale vertical air motions and determining sedimentation rates via detailed microphysical simulations of cloud ice growth and sublimation.

Models are an indispensable part of efforts to assess the climate impact of AIC and explore the effectiveness of associated mitigation options. However, process-oriented model studies relating AIC lifetimes to factors controlling its evolution, such as ice supersaturation, ice microphysics, and dynamical forcing across multiple spatial and temporal scales, are lacking. Therefore, lifetimes vary among studies, from fixed single values (Stuber et al., 2006; Yin et al., 2023) to variability in AIC lifetimes with different mean values and frequency distributions (Newinger & Burkhardt, 2012; Schumann, 2012).

KÄRCHER AND CORCOS 2 of 28

Analysis of satellite-detectable AIC showed e-folding lifetimes typically in the 2 hr range (Vazquez-Navarro et al., 2015). Mean lifetimes inferred from such observations are uncertain, because the detection of old contrails and contrail cirrus suffers from non-linear shape, low optical depth, merging or overlapping with other contrails and cirrus, and low contrast or other unfavorable scene characteristics. Moreover, very young contrails are difficult to identify due to their small width (Driver et al., 2025; Gierens & Vazquez-Navarro, 2018; Minnis, 2003) and parts of older contrails may be advected into the field of view for a short time and falsely characterized as short-lived. Therefore, little is known observationally about the temporal evolution of AIC on regional scales (Kärcher, 2018).

To address the aforementioned knowledge gaps relating to the lifecycle of AIC, we systematically investigate, on the process level, the link between AIC-controlling multiscale meteorological and cloud microphysical factors and AIC lifetime statistics. Section 2 provides details of our approach. Section 3 describes the treatment of physical processes in our model. Section 4 explains our results based on large-ensemble simulations. Section 5 summarizes our main findings, conceptualizes AIC lifetime statistics, and concludes our study by outlining implications for future work.

2. Methods

2.1. Prerequisites

2.1.1. Contrail Initialization

Long-lived contrails are defined as those persisting for at least 10 min after formation (WMO, 2017). In accordance with this definition, we initialize contrails at $t_0 = 10$ min by prescribing shortwave contrail extinction, β , and associated column optical depth, τ , together with a Gamma number-size distribution, $dP/d \ln r$ (normalized to unity) that is associated with a shape parameter, μ , and a mean radius, \bar{r} . We constrain these variables by aircraft measurements. As shown below, this yields the initial contrail vertical depth, δz_0 , and total ice crystal number concentration, n.

Within the contrail, a large number (J=10,000) of simulation ice particles (SIPs) are uniformly distributed (Sölch & Kärcher, 2010). Each SIP contains a number of real ice crystals (multiplicity) and is associated with a minimum number concentration, n_{\min} . All ice crystals in a given SIP have the same physical properties. All SIPs are located above $z_0=11$ km altitude in the midlatitude upper troposphere, defining the lower contrail boundary at a temperature of $T_0=220$ K and a pressure of $T_0=240$ mb. SIP sizes and multiplicities in given radius ranges are drawn from a lognormal distribution with a geometric standard deviation of $T_0=1.5$ and a given mean radius, in line with in situ measurements.

For example, the measured mean values used here, $\beta = 0.0012 \text{ m}^{-1}$, $\tau = 0.27$ (Voigt et al., 2011) and $\bar{r} = 1.5 \,\mu\text{m}$ (Kleine et al., 2018), yield together with $\mu = 3$ the layer depth, $\delta z_0 = \tau/\beta = 225 \text{ m}$, and total number concentration, $n = 61.7 \,\text{cm}^{-3}$. The latter follows from the ratio of total extinction and average extinction per ice crystal:

$$n = \frac{\beta}{\int_0^\infty \pi r^2 Q(r) \frac{dP}{d \ln r} d \ln r},\tag{1}$$

with the Mie extinction efficiency, Q, for small, non-absorbing, spherical ice particles (van de Hulst, 1981) taken at a wavelength of 550 nm. These values represent initial young contrail conditions in the late vortex/early dissipation regime of aircraft wake development (Paoli & Shariff, 2016) as spatial averages across a contrail's cross section perpendicular to the flight direction.

Aviation fuels with fewer soot particle emissions, including biofuels, produce contrails with fewer but larger ice crystals (Kärcher et al., 2015; Paoli et al., 2013). Such a case may be captured by assuming a larger mean radius; for instance, $\bar{r} = 3 \,\mu\text{m}$ leads to $n = 15.5 \,\text{cm}^{-3}$.

2.1.2. Ice Supersaturation

Ice-supersaturated areas constrain AIC persistence. Although the location and duration of ice-supersaturated areas evolve with the synoptic flow, supersaturation does not act as a passive tracer. The production and

KÄRCHER AND CORCOS 3 of 28

maintenance of supersaturation involves vertical air motions. Ice-supersaturated areas have their own spatial and temporal patterns that may or may not be stationary (Irvine et al., 2014; Spichtinger et al., 2005), and patches of subsaturated air may be embedded within them.

The lifetime of ice-supersaturated areas may exceed that of the contrails evolving in them. Occasionally, long contrail lifetimes up to 18 hr were identified (Haywood et al., 2009; Minnis et al., 1998; Vazquez-Navarro et al., 2015), pointing to a significant lifetime variance. Ice crystals can settle out of such regions due to gravity (sedimentation) before large-scale warming and drying sets in or they can leave them due to horizontal advection. Within these areas, ice crystals are also subject to deposition growth (s > 0) or sublimation (s < 0) due to uptake or release of water vapor (H_2O) .

The properties of large-scale ice-supersaturated areas have been investigated using remote sensing (Gettelman et al., 2006; Lamquin et al., 2012; Spichtinger et al., 2003), in situ observations (Diao et al., 2014; Petzold et al., 2020), numerical weather prediction (Reutter et al., 2020), and global climate models (Burkhardt et al., 2008; Lohmann et al., 2008). In addition, Lagrangian trajectory calculations based on large-scale wind fields have been used to quantify origin and duration of ice supersaturation in the upper troposphere (Irvine et al., 2014). The properties of supersaturation fluctuations within these large-scale areas are significantly affected by short-period gravity waves (Kärcher et al., 2023), however the much slower synoptic motions set the baseline temperatures around which these fluctuations occur.

Of special importance for this study is the thickness of ice-supersaturated layers, L. Observations indicate mean values in the range 0.5-1.5 km, associated with large standard deviations that can exceed mean values (Kärcher et al., 2009); smaller vertical thicknesses are more commonly found. In our study, L denotes the total thickness including the contrail.

Another important variable is the ambient H_2O mass mixing ratio, $q_{v,a}$, entrained into contrails. In the present model, this variable is constrained by a prescribed ambient ice supersaturation, $s_a \ge 0$, taken at the ambient temperature at the altitude of the contrail. Analysis of long-term aircraft data revealed exponentially distributed s with a mean value of 0.15 in the upper troposphere, mainly between Europe and North America (Gierens et al., 1999).

Fluctuations in supersaturation, s', relevant for cloud ice microphysics, are generated by fluctuations in temperature, T', that are in turn caused by vertical air motions. The fluctuations are in cloud-free conditions related via (Kärcher & Podglajen, 2019):

$$s' = \frac{\bar{s} + 1}{\bar{T}} \left(\frac{H}{\mathcal{R}_{v} \bar{T}} - \frac{c_{p}}{\mathcal{R}_{a}} \right) T' \equiv \kappa T', \tag{2}$$

where the overbar denotes mean values, H is the latent heat of sublimation, \mathcal{R}_v (\mathcal{R}_a) is the gas constant for water vapor (dry air), and c_p is the isobaric specific heat of dry air. Setting $\bar{s} = 0$ and $\bar{T} = 220$ K yields $\kappa = 0.11$. Typical values of T' in the case of gravity waves lie in the range 0.5-1.5 K (standard deviations), so we expect $s' \approx 0.05-0.15$ in cloud-free upper tropospheric conditions.

Inside a cirrus cloud, s' is reduced (damped) due to ice deposition growth or sublimation and may approach a stationary value depending on the balance between the forcing of fluctuations and their decay. The damping of s is governed by the quenching (phase relaxation) time, τ_q , defined as

$$t_{\mathbf{q}} = \frac{1}{4\pi D n \,\bar{r}},\tag{3}$$

for a pure ice-phase cloud at temperatures below about 225 K where latent heat effects are small (Korolev & Mazin, 2003). In Equation 3, we use the mean ice crystal radius \bar{r} (SIP radii r in our numerical simulations) and the kinetically corrected H₂O diffusion coefficient, $D = D_v \bar{r}/(\bar{r} + \ell)$. Here, $\ell = 4D_v/(\alpha\bar{v})$ is the diffusion length scale, D_v is the molecular diffusivity, and \bar{v} denotes the mean thermal speed of H₂O in air. We employ a constant, particle-average value of the deposition coefficient, $\alpha = 0.1$ (Kärcher et al., 2022). As low s implies low α -values (Lamb & Verlinde, 2011), this choice roughly accounts for the fact that s is constrained to values close to ice saturation in young contrails (Section 3.3). The approach of using constant deposition coefficients is justified

KÄRCHER AND CORCOS 4 of 28

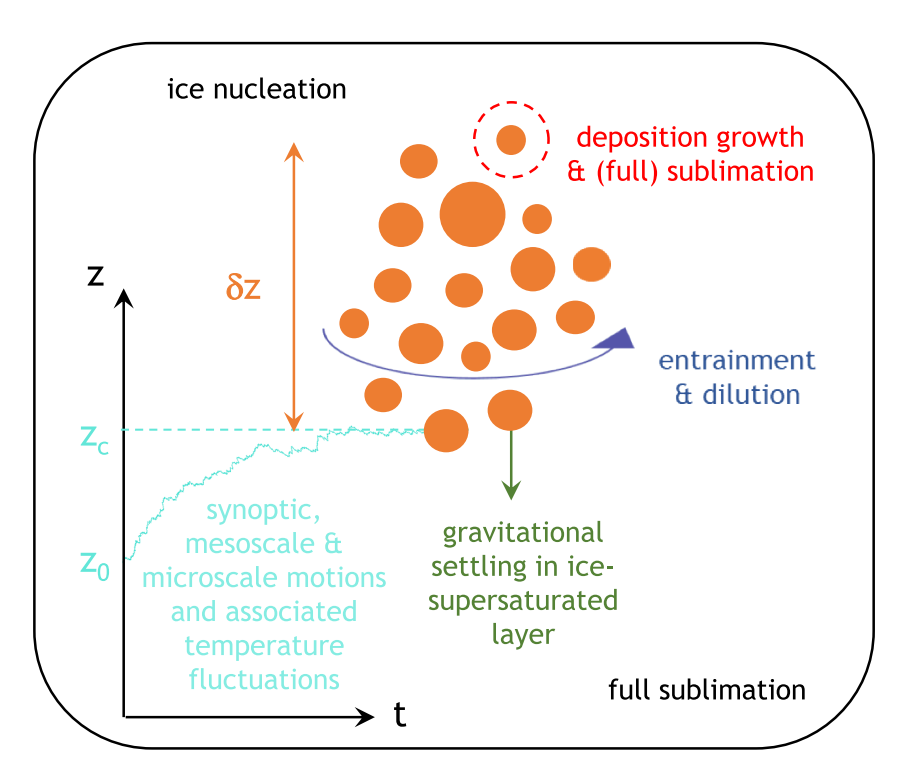


Figure 1. Schematic illustrating the processes controlling Lagrangian vertical motion of, and ice microphysics in, persistent contrails and contrail cirrus as represented in this study.

in simulations of bulk H_2O phase partitioning, as gravity wave motions affect s more significantly than microphysical parameters determining ice growth and sublimation rates (Kärcher et al., 2023). In the case of actively sublimating ice, we set $\alpha = 1$ (Magee et al., 2014).

To first order, the temporal evolution of s inside a cirrus cloud is governed by the generic evolution equation $\dot{s} = (s_0 - s)/t_f - s/t_q$, with the dynamical forcing timescale, t_f (Section 3.3). In steady-state, this implies that s-fluctuations are damped by the factor $t_q/(t_f + t_q)$, yielding

$$s' = \frac{\kappa T'}{1 + t_f/t_q}.$$
(4)

2.2. Conceptual Framework

We devise a dynamical-microphysical simulation model based on a process-oriented description of the key factors affecting AIC lifetimes and microphysical properties. Our model is quasi-one dimensional and contains stochastic elements. As cloudy columns of air, contrails are represented as a subsystem immersed in a larger-scale atmospheric flow. Contrails interact with the air surrounding them via entrainment (Section 3.1). A particle-based description of ice crystal motion and microphysics avoids complications arising from artificial (numerical) diffusion in the computation of crystal positions and radii.

As depicted in Figure 1, the model contrail is represented by a homogeneous vertical layer. The altitude of its lower boundary, z_c , and its thermodynamic and microphysical state are tracked over time in response to a time-dependent vertical wind speed, w, representing synoptic, mesoscale, and microscale motions (Section 3.2). The positions of a large number of SIPs settling due to gravity are tracked individually, allowing us to evaluate its evolving geometrical depth, δz . The upper (lower) contrail boundaries are defined as the altitudes of the highest (lowest) ice crystals.

All SIPs undergo deposition growth and sublimation, continually repartitioning water substance between the gas and particle phase. The air surrounding the contrail is assumed to be at ice saturation or supersaturated with

KÄRCHER AND CORCOS 5 of 28

respect to ice. The air directly above the contrail is assumed to be ice-supersaturated in the case of upward motion (w > 0), potentially allowing ice nucleation to take place. The air at a given distance below the contrail is assumed to be ice-subsaturated, reflecting the vertical extent of ice-supersaturated regions (Section 2.1.2) and causing ice crystals to fully sublimate after settling out of the ice-supersaturated column in which the contrail is evolving.

By simulating the evolution of individual vertical SIP locations and sizes, we account for the fundamental vertical ice crystal sorting known from cirrus cloud measurements (Miloshevich & Heymsfield, 1997). The mechanism by which larger crystals slow the descent of smaller ones higher up in the layer by deposition of supersaturated water vapor is included.

All SIPs are subjected to the same conditions of pressure, temperature, and supersaturation along with the associated fluctuations driven by vertical air motions. Consequently, vertical variations in these variables are not represented. The assumption of vertical homogeneity influences ice crystal positions through their growth histories and size-dependent settling velocities. We note that size sorting of ice crystals can be more pronounced when supersaturation profiles are vertically inhomogeneous. In cases where contrail lifetimes are controlled by sedimentation, it is not straightforward to determine exactly how, and to what extent, lifetimes are affected. This depends on the shape and temporal evolution of the supersaturation profile, the effect of entrainment, and whether the dynamical forcing remains vertically coherent.

Consistent with the assumption of homogeneity in the thermodynamic state, all SIPs experience the same value of w at any time. We account for an idealized synoptic forcing of contrail motion and associated thermodynamic changes. At the mesoscale, rapid temperature fluctuations due to high-frequency gravity waves force the temporal evolution of T and s. Microscale variability in these variables due to isotropic, homogeneous turbulence is also considered. Potential effects of wind shear on AIC lifetimes are not accounted for; they may be limited as long as persistent contrails and contrail cirrus evolve fully embedded within large-scale ice-supersaturated areas, as assumed in this study. Circulations potentially developing inside long-lived AIC as a result of radiative heating, counteracting sedimentation and therefore potentially enhancing lifetimes, are not resolved.

Information about the environment surrounding the contrail is required to simulate entrainment. The contrail moves in a static atmosphere characterized by a constant lapse rate, γ , yielding a linear temperature profile, $T_{\rm a}(z \ge z_0)$. A value of $\gamma = 8$ K km⁻¹ is typical for areas in which contrails evolve (Wilhelm et al., 2022). Ambient air pressure, $p_{\rm a}(z \ge z_0)$, follows from hydrostatic equilibrium. Entrainment affects the temperature and humidity in the contrail and nudges s toward $s_{\rm a}$. Importantly, entrainment leads to a dilution of ice crystal number concentrations. In this study, the ambient air is assumed to be cloud-free.

Inside the contrail, the air is initially ice-saturated, $s_0 = 0$, due to high ice crystal number concentrations (Section 2.1.1). Over time, s varies depending on w and microphysical process rates. Contrail humidity (H₂O mass mixing ratio, q_v), and ice content in SIPs, q_j , are calculated based on a detailed single-particle representation of deposition growth and sublimation (Section 3.5). SIPs are removed from the contrail when q_j vanishes due to full sublimation or when they settle into subsaturated air.

While sedimentation and full sublimation constitute contrail ice crystal loss processes, ice nucleation may provide a source of new contrail ice. This process is unlikely to take place in the contrail area most of the time due to the typically high ice number concentrations, except perhaps in old contrail cirrus with sufficiently low ice crystal numbers or in low-number concentration fall streaks (Section 3.3). However, ice nucleation may occur in clear air right above the top of rising contrails. Therefore, we consider this process (Section 3.6) to study its possible effect on contrail lifetimes.

All simulations are carried out with a time step of $\Delta t = 10$ s to capture effects of rapid temperature fluctuations on cloud microphysics. They start at the end of the contrail formation stage (Kärcher, 2018), meaning that inferred lifetime distributions do not account for contrails less than 10 min of age. Randomness is introduced in the model during initialization of ice crystal sizes and locations, gravity wave forcing, microscale turbulence, and ice nucleation. All simulations are terminated when less than J = 100 SIPs remain; by then, the relative statistical variation of simulated layer properties, $1/\sqrt{J}$, surpasses 10%.

KÄRCHER AND CORCOS 6 of 28

3. Physical Processes

3.1. Entrainment and Dilution

The number concentrations of contrail ice crystals are significantly reduced over time due to dilution caused by entrainment of ambient air. We model entrainment of water vapor and temperature at times $t \ge 0$ past t_0 with the rate $\omega = b/(t_0 + t)$ (Kärcher et al., 2015). The parameter b captures unresolved effects of wind shear and turbulent horizontal diffusion on the contrail width. We define the dilution factor, $\mathcal{D}(t) = \exp[-\int \omega dt]$. Integration over one time step yields the incremental dilution factor, $\mathcal{D} = [(t_0 + t)/(t_0 + t + \Delta t)]^b$.

The temperature and H₂O mass mixing ratio in the contrail after entrainment follow from

$$T(t + \Delta t) = T_{\mathbf{a}} + [T(t) - T_{\mathbf{a}}] \mathcal{D}, \tag{5}$$

$$q_{v}(t + \Delta t) = q_{v,a} + \left[q_{v}(t) - q_{v,a} \right] \mathcal{D}. \tag{6}$$

Assuming the ambient air to be void of ice crystals, the dilution of contrail ice crystal number mixing ratios, $\eta_i = n_i/\varrho$, follows from

$$\eta_i(t + \Delta t) = \mathcal{D}\,\eta_i(t). \tag{7}$$

Values of b may vary during AIC evolution depending on the meteorological situation. A fixed value (0.8) was inferred from in situ measurements during aircraft plume encounters (Schumann et al., 1998) covering all contrail ages including the vortex regime in which dilution is strongly suppressed. Here, we use an average value b=1 to cover AIC evolution after the vortex regime.

3.2. Contrail Forcing and Thermodynamics

The position of the contrail is given by $z_c(t) = z_0 + \int_{t_0}^t w dt$, whereby w is the sum of large-scale and small-scale vertical wind speed components. To avoid limiting contrail lifetimes by large-scale subsidence or horizontal transport, we assume that contrails evolve within a large-scale ice-supersaturated area characterized by a fixed thickness, L. The lifetimes of such regions can reach several days (Irvine et al., 2014), in which contrail clusters have been observed to last longer than 1 day (Bakan et al., 1994).

All temperature changes at time t derived below in this section are added up to obtain the temperature after the next time step. The corresponding pressure changes are derived from the adiabatic law and air density follows from the ideal gas law. These thermodynamic tendencies control contrail microphysics (Section 3.5).

3.2.1. Synoptic Forcing

Concerning the synoptic component, the assumption of a constant vertical wind speed for many hours is not realistic. We therefore model this component as an harmonic oscillation, $w_s(t) = \hat{w}_s \sin(\omega_s t + \varphi_s)$, with peak amplitude $\hat{w}_s = 0.05 \,\mathrm{m \, s^{-1}}$, angular frequency ω_s , period $t_s = 2\pi/\omega_s = 1 \,\mathrm{d}$, and phase φ_s . Choosing $\varphi_s = 0 \,\mathrm{or} \,\pi$ models a full cooling $(w_s > 0)$ or warming $(w_s < 0)$ event over 12 hr, respectively. Choosing $\varphi_s = \pi/2 \,\mathrm{or} \,3\pi/2$ allows us to simulate several shorter consecutive large-scale cooling and warming events.

Assuming that the motion is fast enough so that radiative cooling or heating can be ignored during the lifetime of contrails, the associated temperature change after one time step is given by

$$\Delta T_{s} = -\frac{\Gamma \hat{w}_{s}}{\omega_{s}} \left\{ \sin(\varphi_{s}) \left[\sin(\omega_{s}(t + \Delta t)) - \sin(\omega_{s}t) \right] - \cos(\varphi_{s}) \left[\cos(\omega_{s}(t + \Delta t)) - \cos(\omega_{s}t) \right] \right\}, \tag{8}$$

with the dry adiabatic lapse rate Γ .

3.2.2. Mesoscale Forcing

Although atmospheric motions are dominated by geostrophic turbulence on horizontal scales larger than about 500 km, wind fields are dominated by ubiquitous gravity waves on the mesoscale (Callies et al., 2014). In

KÄRCHER AND CORCOS 7 of 28

particular, analysis of potential and kinetic energy spectra strongly suggests that gravity waves have a leading impact on vertical air motions and resulting temperature fluctuations in the upper troposphere and lower stratosphere (Podglajen et al., 2016). We assume the mesoscale fluctuations to be vertically coherent, that is, the vertical wavelengths exceed the contrail depth. This is motivated by the fact that high-frequency internal waves that are most relevant for our study are associated with long vertical wavelengths (Fritts & Alexander, 2003).

To drive the ice growth and sublimation cycles caused by gravity waves realistically, we model mesoscale vertical wind speed fluctuations, w'_{gw} , as stochastic time series constrained by the standard deviation, σ_w , of autocorrelated, exponentially distributed fluctuations. The resulting temperature fluctuations, T'_{gw} , are constrained by low-frequency damping at a rate f, taken to be the Coriolis frequency, to prevent unphysically large contrail displacements and temperature excursions for lifetimes exceeding 1/f.

The associated change of T'_{gw} , experienced by Lagrangian ice crystals after one time step, is given by Kärcher and Podglajen (2019):

$$\Delta T'_{\rm gw} = -\Delta t \frac{f T'_{\rm gw} + \Gamma w'_{\rm gw}}{1 + f \Delta t},\tag{9}$$

with the fluctuation amplitudes.

$$w_{gw}'(t) = \psi(\bar{w}) \tag{10}$$

$$T'_{gw}(t) = \sum_{i} \Delta T'_{gw}(t - i\Delta t), \tag{11}$$

where the sum runs over all previous time steps and ψ are values drawn from a Laplacian every autocorrelation time, 1/N, with the Brunt-Väisälä frequency, N. The Laplacian, characterized by the mean absolute deviation, $\bar{w} = \sigma_w/\sqrt{2}$, accounts for intermittency in the gravity wave forcing to a degree. We use an average tropospheric value of N = 0.015 rad s⁻¹ and evaluate f at a latitude of 60° , leading to $f = 1.26 \times 10^{-4}$ rad s⁻¹.

3.2.3. Microscale Forcing

After aircraft wake vortices dissipate, the stably stratified background atmosphere impacts vertical air motions (Paoli & Shariff, 2016). Atmospheric turbulence occurring in the upper troposphere is caused by wind shear and convection. For isotropic homogeneous turbulence to affect contrails, the vertical depth of contrails should lie in the inertial range of turbulence. The upper bound of the inertial range is given by the integral length scale measuring the largest distance over which a localized parcel of air is influenced by its previous position. Geometrical thicknesses of persistent contrails, 0.1–1.5 km (Iwabuchi et al., 2012), depend on wind shear and ice supersaturation. Note that contrail thicknesses are in line with thicknesses of ice-supersaturated layers (Section 2.1.2).

One measure of the integral scale is the buoyancy length scale, $l = w_t'/N \approx 10-100$ m, derived from inertial range (Kolmogorov) scaling, where w_t' is a typical wind speed fluctuation due to turbulence. The timescale corresponding to l is given by $l/w_t' = 1/N = \mathcal{O}(1 \text{ min})$. As contrail depths typically exceed l, we cannot safely assume that the whole contrail layer is affected by turbulence in the first place. Regardless, we ignore this limitation and investigate its impact on contrail evolution in a sensitivity study.

Vertical turbulent diffusivity is typically low in the upper troposphere, $D_{\rm t} < 0.1~{\rm m}^2~{\rm s}$, but can increase substantially in patches of air characterized by strong, shear-induced turbulence (Dürbeck & Gerz, 1996). The lifetime of the initial contrail layer against turbulent diffusion is $(\delta z_0)^2/D_{\rm t} > 5.9~{\rm day}$. This means that the effect of vertical turbulent diffusion on contrail depth is much smaller than that of sedimentation (Section 3.4).

 $D_{\rm t}$ scales as $w_t'l$, from which we estimate a typical vertical wind speed fluctuation due to turbulence of $w_t' = \sqrt{D_{\rm t}N}$. With N = 0.015 rad s⁻¹ and $D_{\rm t} < 0.1$ m² s, we get $w_t' < 0.04$ m s⁻¹. The associated temperature and supersaturation fluctuations thus have much smaller mean amplitudes than those generated by gravity waves

KÄRCHER AND CORCOS 8 of 28

(Section 2.1.2). We note that in situations where w'_t is large, we can expect w'_{gw} to be large as well, because turbulence often results from the breaking of gravity waves (Fritts & Alexander, 2003).

We represent the vertical wind speed fluctuations due to turbulence as a stationary, Gaussian stochastic process with standard deviation $\sqrt{D_t N}$ and correlation time 1/N (Abade et al., 2018). The evolution equation for w_t' , and the associated temperature fluctuation change over a time step, $\Delta T_t'$, are given by

$$w_t'(t) = C w_t'(t - \Delta t) + \sqrt{1 - C^2} \sqrt{D_t N} \, \xi, \tag{12}$$

$$\Delta T_t'(t) = -\Gamma w_t' \Delta t,\tag{13}$$

where $C = \exp(-N\Delta t)$ is the correlation coefficient and ξ are temporally uncorrelated Gaussian random numbers with zero mean and unit variance drawn every time step (Bartosch, 2001). The turbulent temperature fluctuations are computed by summing up the respective changes from all previous time steps, $T_t'(t) = \sum_i \Delta T_t'(t - i\Delta t)$.

This a very simplified representation of turbulent velocity fluctuations experienced by contrail ice crystals, which does not account for intermittency. Detailed simulations demonstrate that isotropic turbulence leads to non-Gaussian temperature and ice supersaturation statistics in the inertial range (Kärcher et al., 2025) due to the presence of gradients in T and/or q_v (Warhaft, 2000). Here, we opt to work with a much simpler description, because episodes of strong microscale turbulence in the upper troposphere are rare and, as noted above, only a fraction of the contrail volume may be filled with turbulence.

3.2.4. Contrail Motion

With the information provided in this section, the altitude of the lower contrail boundary, z_c , is evaluated as

$$z_{\rm c} = z_0 + \frac{\hat{w}_{\rm s}}{\omega_{\rm s}} \left\{ \sin(\varphi_{\rm s}) \sin(\omega_{\rm s}t) - \cos(\varphi_{\rm s}) \left[\cos(\omega_{\rm s}t) - 1\right] \right\} - \frac{1}{\Gamma} \left[T'_{\rm gw}(t) + T'_{\rm t}(t)\right]. \tag{14}$$

By assuming that the ice crystals follow z_c apart from sedimentation (Section 3.4), we neglect inertial effects that grow in proportion to particle size. As contrail ice crystals remain typically smaller than most crystals in midlatitude cirrus clouds, this is approximately justified.

3.3. Mesoscale Ice Supersaturation Fluctuations Inside Contrails

By virtue of the described framework, we are now in a position to approximately estimate the evolution of ice supersaturation fluctuations in a persistent contrail due to forcing with ubiquitous gravity waves. Synoptic fluctuations in T have larger amplitudes, but occur on timescales too long to compete with the gravity wave-generated, rapid microphysical processes that quench s in contrails. Microscale fluctuations in T have smaller amplitudes. Thus, the supersaturation fluctuations will primarily be forced by mesoscale variability in T due mainly to short-period gravity waves. An appropriate estimate of the supersaturation forcing timescale is therefore the buoyancy period, $t_f = 2\pi/N$.

In Equation 3, we keep T at 220 K, set \bar{r} to 5 μ m as a rough approximation, and use the initial ice crystal number concentration, 61.7 cm⁻³ (Section 2.1.1), to obtain n(t) from Equation 7. Interpreting the fluctuation amplitudes T' and s' due to gravity waves as standard deviations, we replace T' by the standard deviation of vertical wind speed fluctuations: $\sigma_w = \sqrt{fN}T'/\Gamma$ (Kärcher & Podglajen, 2019), where the harmonic mean gravity wave frequency, \sqrt{fN} , converts temperature into cooling rate fluctuations. Together, this allows us to evaluate the standard deviation of damped s-fluctuations from Equation 4 consistent with the gravity wave forcing (Section 3.2.2).

Figure 2 shows that damped supersaturation fluctuations attain appreciable values a few hours past contrail formation. These results indicate that fluctuations in s driven by gravity waves do not remain strongly damped as contrails mature. It also means that in older contrails and contrail cirrus areas, ice nucleation may occur provided the large-scale forcing leads to a mean supersaturation close to nucleation thresholds for atmospheric ice nucleating particles, that is, $\bar{s} > 0.3$ for mineral dust or > 0.5 for liquid solution droplets from the background

KÄRCHER AND CORCOS 9 of 28

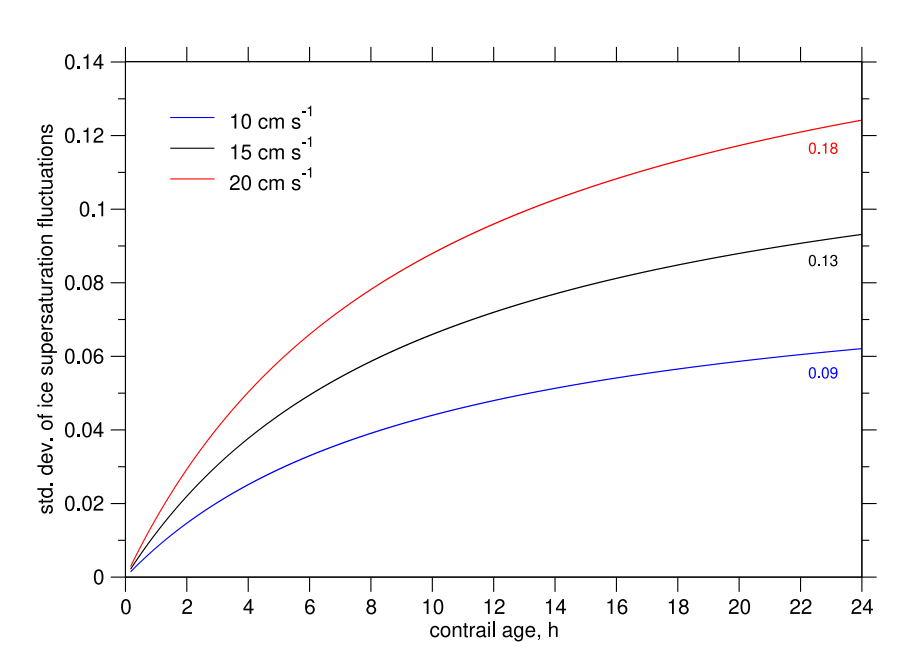


Figure 2. Temporal evolution of the standard deviation of gravity wave-driven ice supersaturation fluctuations inside a persistent contrail for a typical range of mesoscale vertical wind speed fluctuations (legend). Corresponding values in cloud-free air are provided on the right side. Ice crystal number concentration decreases over time due to dilution causing the fluctuation amplitudes to increase with contrail age.

aerosol (Kärcher et al., 2022). Note that the magnitudes of these fluctuations are larger at younger ages in contrails with fewer initial ice crystal number concentrations, see Equation 3.

As fluctuations in s in cloud-free ambient air are larger than inside contrails, ambient cirrus ice crystals may nucleate and get entrained into AIC. This process is not resolved in our model.

3.4. Sedimentation

All SIPs (subscript j = 1, ..., J) are subject to the vertical air motions described in Section 3.2. In addition, their locations are affected by sedimentation.

Terminal fall speeds of small ice crystals with radius r_j are determined by the Stokes relationship, $V_j = [2\varrho g/(9\nu)]C_jr_j^2$, with the mass density of bulk ice, ϱ , and dynamic viscosity, ν , of air, and the gravitational acceleration, g. We account for the transition between the continuum and free molecular regime by correcting the Stokes drag force by the size-dependent Cunningham slip correction, C_i .

The SIP locations inside the moving contrail, Z_i , are thus determined by solving the set of J differential equations,

$$\dot{Z}_i = -V_i,\tag{15}$$

with initial conditions, $Z_{j0} = \delta z_{j0} = z_{j0} - z_0 \ge 0$. Note that in the absence of sedimentation, Z_{j0} -values are conserved during contrail motion. SIPs are removed from the contrail upon settling into subsaturated ambient air. The mean ice crystal location relative to the contrail is given by $\bar{z} = \sum_j Z_j$, and the evolving contrail depth, δz , is determined as the difference between the locations of the highest and lowest ice crystals.

3.5. Deposition Growth and Sublimation

Modeling the evolution of ice supersaturation and ice crystal physical and optical properties requires accurate simulation of crystal growth and sublimation depending on local values of s. In the formulation of these processes, which couple the contrail ice content to the gas phase, a kinetic correction to the H_2O diffusion coefficient accounts for the radial distribution of H_2O from an ice crystal's far field to its surface.

KÄRCHER AND CORCOS 10 of 28

Table 1Description of Simulation Scenarios and Parameter Varied in Each Scenario

Scenario	Description	Section	Parameter
SED	Sedimentation only	4.1	ī
DIL	SED with dilution	4.1	\bar{r}
SYN	Synoptic forcing only	4.2	$arphi_{ m s}$
GW	Gravity wave forcing only	4.3	\bar{w}
GW-SYN	GW with synoptic forcing	4.4	$arphi_{ ext{s}}$
GW-L	GW with different ice-supersaturated layer depths	4.5	L
GW-SA	GW with ambient ice supersaturation	4.6	s_{a}
GW-NUC	GW with ice nucleation	4.7	$R_{\rm n}$
GW-TURB	GW with microscale turbulence	4.8	D_{t}

A total of J+1 equations for $\{q_v,q_j\}$ are solved simultaneously using air temperature and pressure that result from the contrail motion and entrainment. The full microphysical model is defined by the following set of J equations for the ice mass mixing ratios of individual SIPs (Lamb & Verlinde, 2011),

$$\dot{q}_i = 4\pi D_i n_i r_i q_{\text{sat}}(s - S_i), \tag{16}$$

and one additional equation for the H_2O mass mixing ratio, ensuring conservation of total water (apart from losses due to sedimentation):

$$\dot{q}_{v} = -\sum_{i=1}^{J} \dot{q}_{j}. \tag{17}$$

The H₂O mass mixing ratio at ambient ice saturation is denoted by q_{sat} , S_j is the Kelvin correction of q_{sat} directly over the surfaces of radius r_j -particles, and D_j is the kinetically corrected diffusion coefficient for water molecules in air introduced in Section 2.1.2.

3.6. Ice Nucleation

Ice nucleation can occur during upward motion in frontal cirrus clouds, where freshly nucleated ice crystals rapidly settle out of a vertically very shallow nucleation layer, allowing s to stay high right above the cloud top (Kärcher, 2005; Lin et al., 2005). In the present study, we do not specify a nucleation mechanism or explicitly resolve nucleation events, but treat this process parametrically by virtue of a prescribed nucleation rate per unit length of updraft, R_n . Initial radii of freshly nucleated ice crystals are sampled from a Gaussian with a mean radius of $r_n = 1$ µm and standard deviation of $\sigma_n = 0.25$ µm. These crystals are inserted into the contrail slightly below the top depending on their initial fall speed. For example, for a mean gravity wave-induced updraft speed of $\bar{w} = 0.1$ m s⁻¹, $R_n \bar{w} = 6$ ice crystals nucleate per minute for $R_n = 1$ m⁻¹.

New ice is only introduced during periods with w > 0. Whenever the dimensionless number $P = R_n w \Delta t > 1$, we generate P ice crystals with number concentration n_{\min} . If P < 1, we interpret P as a probability of nucleation and generate one ice crystal, but only if a random variate ζ , uniformly distributed between 0 and 1, satisfies $\zeta < P$. If R is chosen too high, ice crystals will accumulate in the layer, probably making it optically thicker than observations would indicate.

We note that this mechanism is unlikely to operate in contrails formed within cirrus clouds. In such cases, entrainment will bring contrail and cirrus cloud ice crystals into contact.

KÄRCHER AND CORCOS 11 of 28

Table 2
Mean Contrail Lifetime and Standard Deviation, Minimum, Maximum, and Median Lifetime for Different Scenarios Taken
From Simulations With an Ensemble Size of 5,000 (Except in Scenarios SED and DIL With 500 Members)

Scenario	Variation	$\bar{t}_{\rm c}~({\rm hr})$	$\sigma_{\rm c}$ (hr)	t_{\min} (hr)	$t_{\rm med}$ (hr)	$t_{\rm max}~({\rm hr})$
SED	$\bar{r} = 1.5 \mu\text{m}$	20.65	0.37	19.76	20.66	21.79
SED	$\bar{r} = 3 \mu \text{m}$	23.25	0.33	22.27	23.24	24.30
DIL	$\bar{r} = 1.5 \mu\text{m}$	20.05	0.33	19.10	20.06	21.16
DIL	$\bar{r} = 3 \mu \text{m}$	16.93	0.30	16.21	16.92	17.77
SYN	$\varphi_{\rm s} = \pi/2$	11.64	0.004	11.63	11.64	11.66
SYN	$\varphi_{\rm s} = 3\pi/2$	0.755	0.001	0.752	0.755	0.758
GW	$\bar{w} = 0.1 \text{ m s}^{-1}$	3.59	3.47	0.37	1.95	15.46
GW	$\bar{w} = 0.15 \text{ m s}^{-1}$	2.64	2.93	0.36	1.14	14.07
GW	$\bar{w} = 0.2 \text{ m s}^{-1}$	2.21	2.57	0.35	0.9	13.96
GW-SYN	$\varphi_{\rm s} = \pi/2$	7.10	5.09	0.36	9.25	11.35
GW-SYN	$\varphi_{\rm s} = 3\pi/2$	0.86	0.54	0.36	0.67	4.43
GW-L	L = 0.225 km	1.72	1.40	0.36	1.09	6.82
GW-L	L = 0.5 km	2.22	2.15	0.36	1.16	10.10
GW-L	L = 1.5 km	2.92	3.88	0.36	1.15	17.51
GW-SA	$s_{\rm a} = 0.05$	4.87	4.34	0.36	3.62	16.45
GW-SA	$s_a = 0.1$	7.48	5.23	0.37	8.23	16.51
GW-SA	$s_{\rm a} = 0.15$	9.40	6.13	0.37	10.66	16.56
GW-NUC	$R_{\rm n} = 1 \text{ m}^{-1}$	3.19	3.86	0.35	1.2	21.5
GW-NUC	$R_{\rm n} = 5 \text{ m}^{-1}$	4.32	6.43	0.36	1.2	>30
GW-TURB	$D_{\rm t} = 0.05 \; {\rm m}^2 \; {\rm s}^{-1}$	0.98	1.08	0.36	0.62	13.2
GW-TURB	$D_{\rm t} = 0.1 \; {\rm m}^2 \; {\rm s}^{-1}$	4.93	5.79	0.36	1.11	19.5

Note. The duration of the unresolved contrail formation stage (10 min) is added to all simulated lifetimes.

4. Results

Key features of each scenario are summarized in Table 1. Recall that contrail lifetimes are determined as the point during contrail evolution when just 100 SIPs are left and that we add 10 min of contrail age, the duration of the unresolved contrail formation stage, to obtain the full lifetime.

We summarize the values of parameters that are not varied: $J=10^4$, $\mu=3$, $\sigma_r=1.5$; $\delta z_0=225$ m, $t_0=10$ min, $z_0=11$ km, $T_0=220$ K, $p_0=240$ mb, $s_0=0$; b=1, $\gamma=8$ K km⁻¹; $\hat{w}_s=0.05$ m s⁻¹, $t_s=1$ d; N=0.015 rad s⁻¹, $f=1.26\times 10^{-4}$ rad s⁻¹; $\alpha=0.1$; $r_0=1$ μ m and $\sigma_0=0.25$ μ m.

From the ensemble of simulations, we generate probability density functions of AIC lifetimes. Lifetime statistics for all scenarios are summarized in Table 2 and Figure 3.

4.1. Sedimentation and Dilution

We start by estimating the maximum time it takes for a monodisperse contrail ice crystal population (constant radius \bar{r}) to settle through the initial contrail (depth δz_0) in static conditions (w = 0). This time is given by $\delta z_0/V(\bar{r}) \approx 7.2$ (1.9) days for $\bar{r} = 1.5$ (3) µm. If we allow the same particles to additionally sediment through ice-supersaturated air of depth $L-\delta z_0$ below the contrail, the settling times are correspondingly longer. These simple estimates do not account for a polydisperse population and crystal size changes due to ice microphysical processes.

Scenarios SED and DIL explore the lifetimes of a size-dispersed population with gravitational settling alone, that is, without contrail motion and associated temperature changes, and ice nucleation, but include ice crystal growth and sublimation. We prescribe $\bar{r}=1.5\,\mu\mathrm{m}$ and $L=\delta z_0=225\,\mathrm{m}$ so that the ice crystals are removed from the

KÄRCHER AND CORCOS 12 of 28

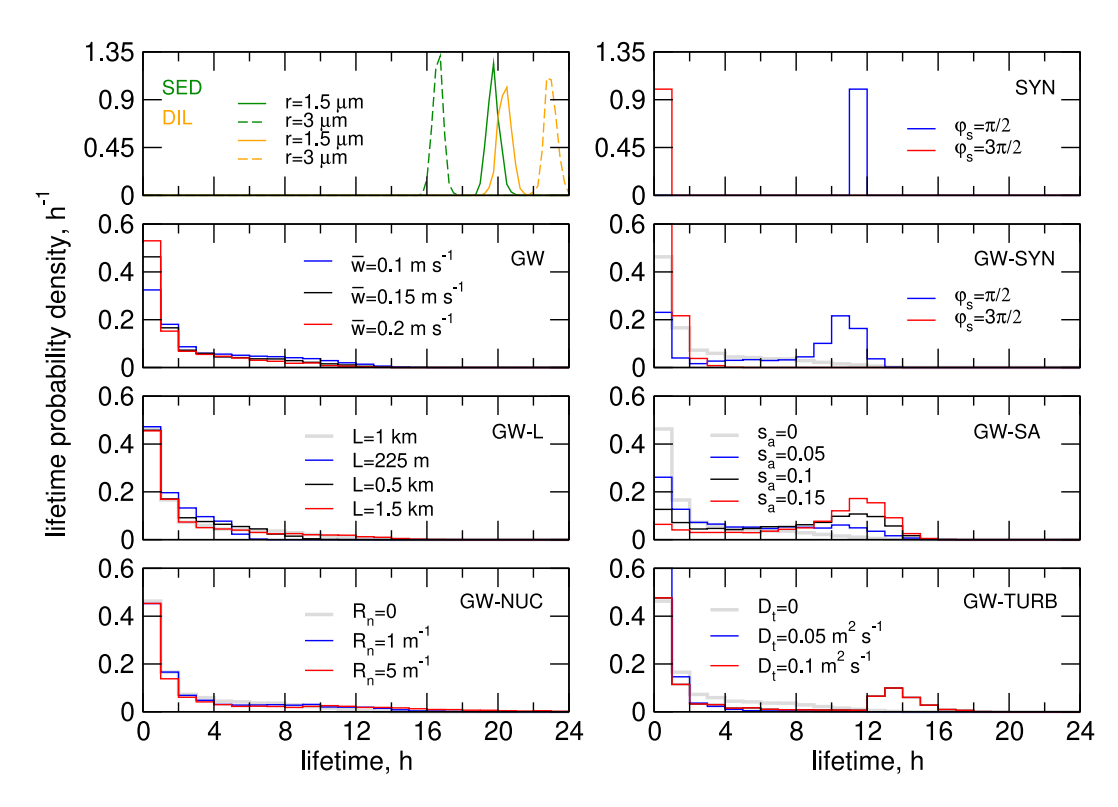


Figure 3. Contrail lifetime statistics for different scenarios. For ease of comparison, gray curves repeat the statistic from scenario GW for $\bar{w} = 0.15 \text{ m s}^{-1}$. The bin width to generate the statistics is 1 hr, except in SED and DIL where a finer grid is used.

contrail immediately after falling out of the initial layer, as in the above settling estimates. Note that although the contrail is initialized at ice saturation, supersaturation directly over a curved particle surface is negative due to the higher H_2O saturation vapor pressure (Lamb & Verlinde, 2011). Therefore, growth and sublimation may affect ice crystals in these otherwise static scenarios.

We continue by examining the scenario SED, where no entrainment and dilution occurs. The mean lifetimes and their standard deviations simulated for two different initial mean radii are noted in Table 2. The associated probability density distributions (PDFs) are shown in Figure 3. The minor spread in lifetimes is caused by randomly choosing initial ice crystal sizes and locations (Section 2.1.1). More importantly, the simulated lifetimes in scenario SED are much shorter than the above monodisperse estimates indicate.

The substantial decrease in lifetimes is caused by a combination of two factors. (1) There is a spread in ice crystal sizes and to a good approximation, the terminal fall speed scales αr^2 . Although it takes longer time for smaller ice crystals close to the contrail top to settle into subsaturated air, large crystals in the population close to the lower contrail boundary quickly leave the contrail. (2) The Kelvin effect drives sublimation of small ice crystals. Full sublimation increases q_v and drives deposition growth of large ice crystals, which in turn accelerates sublimation. This mass transfer of water substance across phases is reminiscent of the Wegener-Bergeron-Findeisen mechanism (Lamb & Verlinde, 2011) and has been identified as a critical factor in the evolution of young contrails (Lewellen et al., 2014) and anvil cirrus (Jensen et al., 2024). Taking (1) and (2) together, this means that initially small ice crystals have less potential to prolong the overall lifetime.

To illustrate this explanation for $\bar{r} = 1.5 \,\mu\text{m}$, we analyze results taken from one statistical realization in greater detail; note that results between different ensemble members are similar due to the small statistical spread of lifetimes in this scenario. Specifically, we show in Figure 4 the initial ice crystal size distribution, along with distributions at 10 hr midway through the contrail evolution and at 20 hr at the end of its evolution (solid curves).

In the initialized size distribution, contrail ice crystals with radii >5 μ m are basically absent. After 10 hr, the total number concentration, measured by the area under the distribution, has decreased considerably due to sublimation

KÄRCHER AND CORCOS 13 of 28

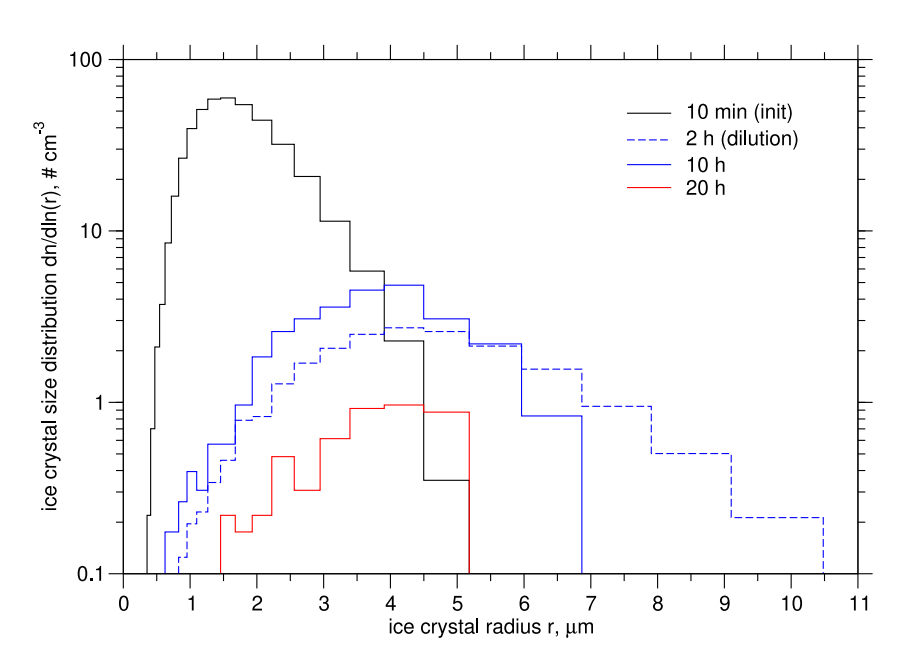


Figure 4. Contrail ice crystal size distributions for $\bar{r} = 1.5 \,\mu\text{m}$ (solid curves) without accounting for dilution (scenario SED) at ages 10 hr (blue) and 20 hr (red) and (dashed blue curve) with dilution (scenario DIL) at 2 hr. The initial distribution (solid black curve) at 10 min is also shown.

of the smallest crystals. The resulting vapor growth has produced ice crystals up to about $7 \,\mu m$ of radius, enhancing the distribution spread. At 20 hr, only a few ice crystals are present in the narrow radius range $2-5 \,\mu m$. In this scenario, ice crystals in this size range are neither strongly affected by sublimation nor do they sediment rapidly out of the contrail.

Dilution reduces the contrail ice number concentration very rapidly. To address this point, we simulated the same scenario with dilution (b = 1). Recall that dilution goes along with entrainment of H_2O , at this point assuming ice-saturated ambient air and slightly warmer temperatures (Section 3.1).

We show in Figure 4 one ice crystal size distribution affected by dilution after 2 hr (dashed curve). This distribution is comparable to the one taken at 10 hr without dilution in terms of total ice number concentration, but extends to radii up to only about $10\,\mu m$ before settling out and produces a large distribution spread. The appearance of such large ice crystals is caused by the diminishing ice concentrations, allowing a comparable amount of H_2O mass to be distributed among fewer crystals. This result underscores the strong impact of dilution in young contrails and highlights the nonlinear interaction with ice microphysics.

To complete this discussion, we examine in scenario DIL the lifetime results obtained with dilution, again for two different values of \bar{r} . The mean lifetimes for $\bar{r}=1.5\,\mu\mathrm{m}$ in the cases with and without dilution are very similar ($\approx 20\,\mathrm{hr}$, Table 2). To understand this, we show in Figure 5a the evolution of the total number of SIPs, J, in the simulations along with the number of sublimated and sedimented SIPs. In both cases, a large number of the initially 10,000 SIPs sublimates due to the Kelvin effect. Without dilution (solid curves), many SIPs sublimate within the first 2 hr, whereas sedimentation notably depletes SIPs much later. With dilution (dashed curves), sublimation losses are smaller and sedimentation losses are larger. Nonetheless, mean lifetimes are comparable. In both cases, an ice mode around 4 $\mu\mathrm{m}$ remains after 20 hr and only 100 SIPs are left, corresponding to a total ice crystal number concentration of about 0.6 (0.005) cm⁻³ without (with) dilution.

The mean lifetime for larger $\bar{r}=3\,\mu\mathrm{m}$ is 2.6 hr longer than for $\bar{r}=1.5\,\mu\mathrm{m}$ without dilution, whereas it is 3.12 hr shorter with dilution. To explain this, we show Figure 5b simulated SIP numbers for $\bar{r}=3\,\mu\mathrm{m}$. As expected, J_{sub} is smaller and J_{sed} is larger with dilution due to on average larger crystals, cp. with Figure 5a. The sedimentation losses are large enough (removing about 86% of all SIPs) to terminate the contrail earlier than for $\bar{r}=1.5\,\mu\mathrm{m}$, where only short of 50% of all SIPs are lost by settling.

KÄRCHER AND CORCOS 14 of 28

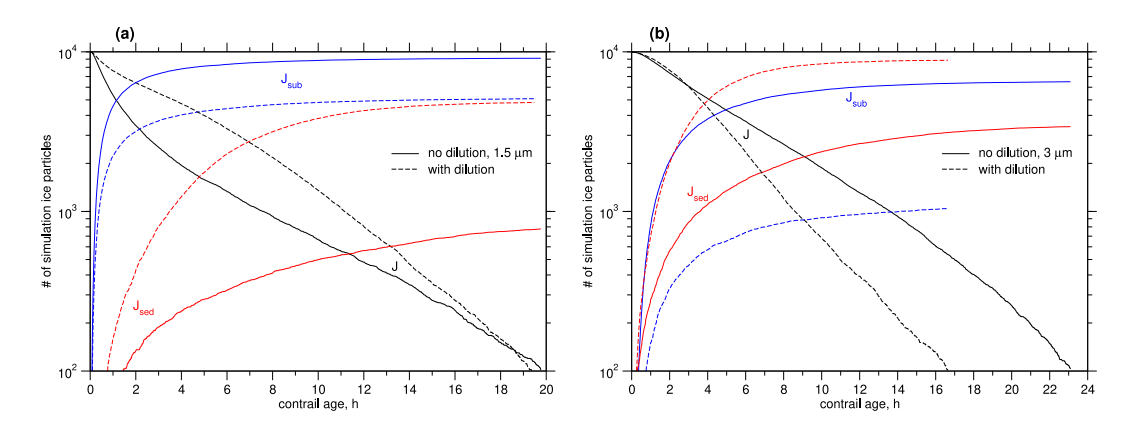


Figure 5. Temporal evolution of the total number of simulation ice particles (black curves), along with the number sublimated (blue) and sedimented (red) for simulations in scenario SED without (solid) and with (dashed) dilution for (a) $\bar{r} = 1.5 \,\mu\text{m}$ and (b) $\bar{r} = 3 \,\mu\text{m}$. Contrail age denotes time past 10 min.

4.2. Synoptic Forcing

Scenario SYN examines changes relative to DIL with $\bar{r} = 1.5 \,\mu\text{m}$ caused by synoptic forcing. Note that the Kelvin effect, sedimentation, entrainment of ice-saturated air, dilution, and their complex interaction as described in Section 4.1 continue to be accounted for. We set $L = 1 \, \text{km}$ to additionally allow for a column of 775 m of ice-supersaturated air below the contrail.

We select two wave phases to mimic subsequent cooling and warming events (Section 3.2). The case with phase $\varphi_s = \pi/2$ starts with cooling that lasts 6 hr, followed by a prolonged 12 hr-warming, and ends with a 6 hr-cooling period. The case with phase $\varphi_s = 3\pi/2$ starts with warming that lasts 6 hr, followed by a prolonged 12 hr-cooling and ends with a 6 hr-warming period.

For both wave phases, mean lifetimes are significantly lower than in all SED scenarios due to the warming periods that drive enhanced sublimation losses. Note that due to H_2O diffusion, sublimation rates increase with decreasing ice crystal sizes. Thus, the effect is particularly strong when the warming occurs early ($\varphi_s = 3\pi/2$), that is, when ice crystal sizes are small and sedimentation is very inefficient.

The lifetime distribution peaks around 11.6 hr mean lifetime when the contrail starts off with a cooling event $(\varphi_s = \pi/2)$. In this case, ice crystals grow to radii of up to $\approx 15 \,\mu m$ at which point they settle quickly through the ice-supersaturated layer below the contrail into ice-subsaturated air. The location of the lifetime peak correlates with the supersaturated layer depth: smaller (larger) L leads to smaller (larger) maximum radii and thus shorter (longer) mean lifetimes. We expect that using a forcing history that more realistically mimics the synoptic situation would blur this peak.

4.3. Mesoscale Forcing

Scenario GW focuses on how gravity waves alone alter contrail lifetimes relative to a static situation for three representative values of \bar{w} . Otherwise, these simulations with $\bar{r} = 1.5 \,\mu\text{m}$, b = 1, $s_a = 0$, and $L = 1 \,\text{km}$ are identical to scenario SYN. Initially, the initial mean ice crystal size increases rapidly as described in Section 4.1.

The random nature and rapidity of mesoscale temperature fluctuations results in remarkably broad lifetime statistics. This feature is consistent with observations (Section 4.9). Contrary to pure synoptic forcing, the spread in lifetimes is comparable to the mean values. Mean and maximum lifetimes decrease with increasing \bar{w} . Remarkably, maximum lifetimes reach up to 15.5 hr without imposing ambient ice supersaturation. This is due to the fact that for extended time periods, the gravity wave forcing stabilizes the contrail ice crystal size distribution due to rapid succession of moderate amplitude sublimation and growth events. When ice crystals grow to sufficiently large sizes, they are less likely to fully sublimate in warming periods. In such cases, long lifetimes are related to the time ice crystals need to fall out of the ice-supersaturated layer.

The marked increase of the statistic toward young ages, especially in cases with larger \bar{w} , is due to the fact that the gravity wave-generated fluctuations in s occur in the presence of still small ice crystals. The attained level of

KÄRCHER AND CORCOS 15 of 28

subsaturation suffices to quickly dissolve contrails by full sublimation. We expect that larger (smaller) initial \bar{r} would decrease (increase) sublimation rates; according to the discussion in Section 4.1, the associated ice crystal losses, and thus, lifetimes, are sensitive to \bar{r} .

Because scenarios without gravity wave activity do not appear to be realistic, we continue this discussion by combining mesoscale forcing (based on $\bar{w} = 0.15 \text{ m s}^{-1}$) with other forcings and processes.

4.4. Combining Mesoscale With Synoptic Forcing

Scenario GW-SYN explores how gravity wave activity affects AIC lifetime statistics in the presence of the idealized synoptic forcing.

We find a strong sublimation effect due to initial warming ($\varphi_s = 3\pi/2$), resulting in a statistic with a low mean lifetime due to the dominant influence of sublimation. The distribution spread is mainly caused by the added mesoscale variability.

In the opposite case with an initial cooling phase $(\varphi_s = \pi/2)$, we find a size selection effect similar to scenario SYN, because growth and sedimentation are more relevant, resulting in a distribution with a ≈ 7 hr lifetime peak. This statistic is still left skewed due to wave-induced sublimation events.

4.5. Varying the Depth of the Ice-Supersaturated Layer

Scenario GW assumed a total ice-supersaturated layer depth of L=1 km together with the initial contrail depth of $\delta z_0=225$ m. This means that once ice crystals fall out of the initial contrail, they can still fall a distance $L-\delta z_0=775$ m before entering ice-subsaturated air and being removed from the contrail.

Scenario GW-L describes results based on ± 500 m changes in L. Since δz_0 is not changed, these cases correspond to a shorter (225 m for L=0.5 km) or longer (1,225 m for L=1.5 km) distance below the contrail a falling ice crystal can survive. In both cases, the lifetime distributions are very similar. However, for L=0.5 km, the maximum lifetime decreases by almost 4 hr. For L=1.5 km, one ensemble member has a lifetime >4 d, suggesting that variability in deep ice-supersaturated layers can create ice crystals in the right size range occasionally leading to very long survival times.

The third simulation with $L = \delta z_0$ mimics a very shallow ice-supersaturated layer equal to the initial contrail depth. Consequently, mean, medium, and maximum lifetimes are smaller than for L = 0.5 km, representing lower-limit values for this scenario.

4.6. Entraining Ice-Supersaturated Air

Scenario GW-SA is identical to scenario GW where $s_a = 0$, but allows the entrained ambient air to be ice-supersaturated with $s_a > 0$.

For $s_a = 0.05$, enhanced ice crystal growth offsets sublimation losses that occurred with entrainment of ice-saturated air in scenario GW and produces contrails with an about 1 hr longer mean lifetime. With increasing s_a , lifetimes peak in a broad range between 8-14 hr at the expense of younger contrail ages, further increasing mean lifetimes and their spread. Maximum lifetimes are around 16.5 hr in all cases. These lifetimes are obtained for the baseline value L = 1 km.

Further increases of s_a do not necessarily cause longer-lived contrails due to enhanced sedimentation. We refrain from choosing ice supersaturation larger than 0.15, as prescribing such large constant values for the entire lifecycle may not be realistic.

4.7. Ice Crystals Nucleating at the Top of Contrails

Including ice nucleation at the top of rising contrails in the scenario, GW-NUC, leads to effects similar to entraining ice-supersaturated air. Lifetime maxima happens to be sensitive to the prescribed SIP production rate per unit updraft, R_n . Here the transition from a broad distribution to a lifetime peak develops for nucleation rates exceeding about 1 m⁻¹. We find substantial increases in mean lifetime and associated spread for $R_n = 5 \text{ m}^{-1}$.

KÄRCHER AND CORCOS 16 of 28

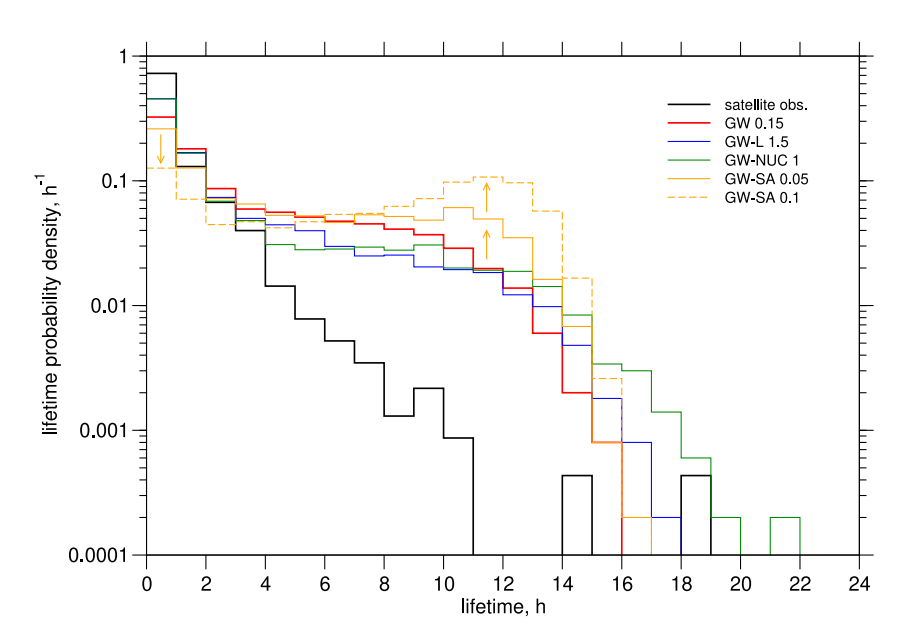


Figure 6. Probability distribution functions of contrail lifetimes from satellite remote sensing observations in comparison with selected statistics repeated from Figure 3. The observed (black) and simulated baseline (red) distributions are highlighted with thicker stair steps.

4.8. Combining Mesoscale With Microscale Forcing

Scenario GW-TURB is identical to scenario GW, but additionally includes low-amplitude turbulent temperature fluctuations. These fluctuations either enhance or diminish the effect of mesoscale fluctuations, increasing or decreasing the mean lifetime and lifetime spread relative to GW, depending on the choice of the vertical diffusivity, D_t . As values <0.1 m² s are rare in the upper troposphere (Section 3.2.3), effects of turbulence are on average likely small.

4.9. Comparison With Observations

Only satellite observations provide sufficient statistical data to compare with our model results. However, as noted in Section 1, direct comparison is not straightforward, because satellite-derived contrail lifetime statistics are affected by a number of sampling issues. We choose scenarios without synoptic motions in this comparison to avoid large-scale dynamical lifetime limitations.

The lifetime statistic derived from 2,305 contrails identified by the Automatic Contrail Tracking Algorithm (ACTA) is shown in Figure 6 (Vazquez-Navarro et al., 2015). The underlying measurements have been taken over Europe and the North-Atlantic flight corridor using information from the Meteosat Second Generation satellite. The inferred statistic of lifetimes of satellite-detectable contrails is plotted together with several simulated statistics, from which we select as the baseline the one predicted by gravity wave forcing only (GW), assuming an average forcing amplitude ($\bar{w} = 0.15 \text{ m s}^{-1}$), ice-saturated ambient air ($s_a = 0$), and a deep ice-supersaturated layer (L = 1 km) that includes the contrail. Moreover, we compare with the above sensitivity studies increasing the values of L (Gw-L), R_n (GW-NUC), and s_a (GW-SA).

One feature of the observed statistic is common to all simulation scenarios: the spread in contrail lifetimes is similar to or larger than the mean value, which by itself has important ramifications for AIC RF and mitigation (Newinger & Burkhardt, 2012). Although the initial rapid drop in lifetimes predicted in most scenarios due to gravity wave activity is roughly in line with the observations, all simulated statistics show a much larger number of contrails with ages exceeding 4 hr. These contrails escape detection either because they do not retain their linear shape or their optical depth falls below the ACTA detection limit (≈ 0.1).

As the remote sensing measurements cannot detect narrow, young contrails, the initial contrail lifetime is unknown and the large number of very young contrails with ages up to about 30 min may be a measurement artifact. For instance, long-lived contrails that are lost during tracking and therefore detected only in a small period of time

KÄRCHER AND CORCOS 17 of 28

may be falsely associated with a small age. Therefore, the mean lifetime of 0.91 hr is a lower limit. Gierens and Vazquez-Navarro (2018) estimate that the actual mean lifetime of ACTA contrails may be three times longer, that is, amounts to about 2.7 hr. According to Table 2, this is basically identical to the mean lifetime we compute in scenario GW (2.64 hr). The ice-supersaturated scenarios GW-SA predict significantly longer mean values (4.87 hr for $s_a = 0.05$ and 7.48 hr for $s_a = 0.1$). The latter is likely caused by assuming constant s_a -values over many hours minimizing sublimation losses.

Older persistent contrails and contrail cirrus are underrepresented in the ACTA data set and consequently, the probability of finding long lifetimes is underestimated. The fact that the two cases with observed lifetimes slightly exceeding 14 and 18 hr lie within the tail of all simulated statistics strongly suggests that our model captures the physical processes necessary to explain such long lifetimes and that in nature more long-lived contrails exist than the ACTA data indicate. Conversely, models that fail to reproduce very long-lived AIC do not properly capture the underlying lifetime-controlling processes.

An in-depth analysis of the observed statistic suggests a tendency of AIC to survive the longer, the older they are (Gierens & Vazquez-Navarro, 2018). Therefore, physical mechanisms and processes that prolong AIC lifetimes (Table 2), such as deep ice-supersaturated layers, entrainment of moderately ice-supersaturated air, and perhaps ice nucleation and microscale turbulence, can be more influential the longer contrails exist.

The tendency of the simulated statistics from scenarios GW-SA to show fewer occurrences with less than 4 hr lifetime and more long-lived contrails (ages $\approx 8-14$ hr) with increasing s_a (arrows in Figure 6) is in line with a conceptual lifetime model developed to interpret climate model results (Newinger & Burkhardt, 2012). The conceptual model predicts in ice-supersaturated areas fewer contrails with ages below 4 hr than found here, as it does not account for mesoscale variability in vertical wind speeds, thereby underestimating sublimation losses similar to the climate model.

5. Discussion

We have introduced and presented results from a model suitable for the estimation of lifetimes of persistent contrails and contrail cirrus. Its development is based on a detailed representation of underlying processes, which is generally key for a reliable assessment of performance and predictive capability of AIC models. In our model, deposition growth, sublimation, and sedimentation are accurately tracked on a per-particle level. The simulated contrails evolve in large-scale ice-supersaturated areas to prevent lifetime limitations due to subsidence or advection into ice-subsaturated air. Parameters driving the physical processes are vertical wind speeds quantifying the strength of dynamical forcing across multiple scales, vertical extent of ice-supersaturated layers, magnitude of ice supersaturation in air entrained into contrails, ice nucleation rate at contrail tops, and turbulent vertical diffusivity.

5.1. Summary of Main Results

In scenarios without vertical wind forcing, we have identified an intricate interplay between dilution and cloud ice microphysics that may impact AIC evolution by altering the ice crystal size distribution shortly after the formation stage.

Synoptic warming occurring early after contrail formation can limit mean contrail lifetimes to less than a few hours. Sharp lifetime peaks seen in scenarios that include only synoptic forcing will be flattened out when variability in the idealized forcing history and in ice-supersaturated layer depths would be accounted for.

Mesoscale temperature fluctuations induced by gravity waves lead to a wide range of AIC lifetimes by inducing rapid ice crystal growth and sublimation cycles. Adding such mesoscale variability brings the simulated lifetime statistics in general agreement with observations that exhibit a large relative dispersion (spread divided by mean value) of contrail lifetimes. The efficiency by which wave-induced variability in ice supersaturation affects AIC lifetimes depends, among other factors, on the mean size of contrail ice crystals right after formation.

Especially in ice-saturated conditions, gravity wave activity leads to a selection of contrail ice crystal sizes. Only those remain that on the one hand are large enough to escape full sublimation and on the other hand small enough to remain in the ice-supersaturated layer. Preferred crystal radii are typically near $10\,\mu m$ in 1 km thick ice-supersaturated regions at main cruising altitudes and around 220~K.

KÄRCHER AND CORCOS 18 of 28

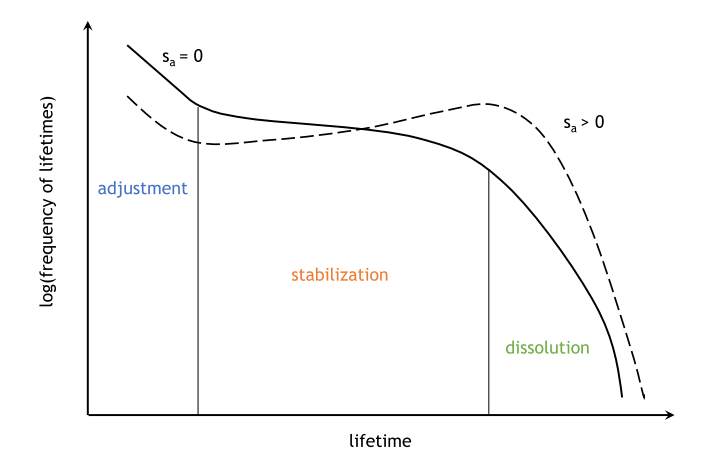


Figure 7. Schematic lifetime frequency distributions of persistent contrails and contrail cirrus indicating three major evolutionary regimes. The solid (dashed) curve represents an equilibrium (ice-supersaturated) environment in which AIC evolves. The wide range of lifetimes is caused by gravity wave activity leading to a selection of preferred ice crystal sizes promoting contrail longevity. Maximum lifetimes increase in thicker ice-supersaturated layers or in the presence of enhanced small-scale turbulence and ice nucleation

Entrainment of moderately ice-supersaturated air favors the generation of long-lived contrails (ages around 12 hr) and at the same time reduces the number of shorter-lived ones (ages <1-2 hr). The main reason is that enhanced deposition growth leads to larger ice crystals, hence, reduced sublimation losses. Periods of more strongly ice-supersaturated entrainment of air may increase the sizes of ice crystals further and may thus prevent long AIC lifetimes due to enhanced sedimentation losses.

Further parameters affecting lifetimes include the depth of ice-supersaturated layers, new ice crystal formation in air right above rising contrails, and microscale turbulence. Increasing the layer depth and ice crystal nucleation may cause very long lifetimes (18–22 hr). Although it is unclear how much of a contrail layer is affected by turbulence, effects of associated supersaturation fluctuations remain limited except perhaps in situations with large vertical diffusivity. These processes are only crudely represented here and require further study with more comprehensive models.

Observed contrails have occasionally been associated with very long lifetimes (Haywood et al., 2009; Minnis et al., 1998; Vazquez-Navarro et al., 2015). This increases confidence in our model framework, as it captures the suite of physical processes needed to explain such long-lived contrails. According to our study, these must be considered rare and possibly require an interplay between weak (if any) synoptic warming, moderate gravity wave activity, and

moderately ice-supersaturated regions with deep layers, possibly aided by ice nucleation and microscale turbulence.

5.2. A Fresh Look on AIC Lifetime Statistics

Figure 7 summarizes the salient features of AIC lifetime statistics and augments the limited knowledge on the transition of contrails into cirrus clouds obtained from in situ observations (Schröder et al., 2000). Three evolutionary regimes can be conveniently defined with a focus on microphysically controlled lifecycles according to scenario GW (i.e., excluding large-scale lifetime limitations).

In the initial adjustment regime, which develops alongside or after aircraft wake dissipation, the combined effects of vertical wind forcing, dilution of ice crystal number concentrations, and wave-driven deposition growth and sublimation of ice crystals (Figure 4) produce a substantial number of contrails with relatively short (<4 hr) lifetimes. The occurrence of these short-lived contrails decreases significantly when ice-supersaturated air is entrained (Figure 3). In this regime, most contrails are expected to be linear in shape. However, only a subset of persistent contrails can be detected in satellite imagery because of their narrow width (Gierens & Vazquez-Navarro, 2018). This limitation makes it difficult to attribute individual contrails to the specific flights that have caused them.

In the subsequent stabilization regime, maturing contrails respond to changing atmospheric conditions in large-scale ice-supersaturated regions. Mesoscale temperature fluctuations and magnitude of ambient ice supersaturation primarily control the rate of selection of preferred ice crystal sizes from the size distribution due to cycles of deposition growth and sublimation that become increasingly kinetically controlled with time. The efficiency of size selection shapes the exact functional form of the lifetime statistic and the survival of ice crystals escaping both full sublimation and sedimentation allows for >4 hr lifetimes (Figure 6).

In nature, this intermediate stage allows for merging of individual contrails, their transition into irregularly shaped contrail cirrus, and interactions with natural cirrus, significantly impeding the estimation of associated RF. Together with the fact that in this stage AIC becomes increasingly optically thin, this means that a significant fraction of persistent contrails and contrail cirrus escape detection by satellites (Kärcher et al., 2009). The mean optical depth derived from such a limited data set is therefore underestimated and no longer a good proxy for RF (Kärcher et al., 2010). Note that despite the relatively rare occurrence of long-lived AIC, their RF may be significant because they are associated with large horizontal coverage (Burkhardt & Kärcher, 2011).

KÄRCHER AND CORCOS 19 of 28

AIC lifetime can, at any stage, be limited by large-scale subsidence or horizontal transport of contrails into ice-subsaturated air (Hofer & Gierens, 2025). If this does not happen, we enter the final dissipation regime, where substantial ice crystal losses occur, either by sedimentation or sublimation. In the former case, the time of its onset is impacted by the thickness of ice-supersaturated layers (Figure 3 and Table 2), along with the mean size the contrail ice crystals achieved. Furthermore, the duration of the dissipation regime extends over a few hours because of the size spread characterizing the ice crystal size distribution. It is narrower only when rapid warming events dissolve the contrail.

Tracking of contrails by satellites alone does not allow one to determine the processes that end the lifetime. Future work may quantify the relative importance of sedimentation and sublimation in dissolving contrails, which presumably depends on the large-scale flow. We illustrate the evolution of an ice crystal number-size distribution of a contrail dissolving by sedimentation from our baseline scenario GW in Appendix A (Figure A1).

5.3. Implications for Contrail Modeling

Presumably, large-scale subsidence is unlikely to occur right after persistent contrails are generated. It would be interesting to study where and how often such meteorological situations actually occur; atmospheric effects of AIC within them would be small.

Mesoscale variability and associated microphysical changes have not been included in past analyses of contrail lifetimes (Hofer & Gierens, 2025). Moreover, contrail ice crystal mean size and size spread have rarely been discussed in AIC parameterizations or models. We therefore suggest that AIC models, including large-eddy, cloud-resolving, and global simulations, consider gravity wave forcing along with proper microphysical modeling of ice growth and sublimation. Including only synoptic motions and sedimentation is not sufficient to predict AIC lifetimes with confidence.

The representation of diffusive and kinetic limitations to ice crystal growth and the inclusion of high-frequency internal gravity wave forcing in our model is a significant advantage over a widely used, empirical contrail model that is based on preliminary relationships containing a large number of freely adjustable parameters (Schumann, 2012). The latter model replicates satellite observations of AIC mean lifetime and optical depth, but those inevitably suffer from selection biases. This is accomplished by (a) tuning heuristic ice crystal loss rates without reference to ice supersaturation, (b) applying saturation adjustment to ice growth ignoring fundamental microphysical growth timescales, and (c) representing sedimentation of the contrail center of gravity instead of ice crystal settling distorting the full fallstreak behavior of cirrus clouds. Such an approach cannot be expected to yield robust results in meteorological conditions that differ from those used to define the set of model parameters.

In fact, a recent intercomparison between the contrail plume model by Schumann (2012) and a higher-fidelity plume model based on Fritz et al. (2020) revealed significant and fundamental differences in predicted contrail optical depth and lifetime, implying that mitigation of AIC RF via contrail avoidance may have a poorly quantified outcome (Martinez et al., 2025), in support of previous arguments (Lee et al., 2023).

We caution that growth efficiencies of ice crystals, encapsulated in deposition coefficients that depend on temperature, pressure, ice supersaturation, and ice crystal size, are not well understood below 240 K (Rui et al., 2025). A distribution of deposition coefficients within contrails and the associated development of non-spherical ice crystal habits may impact sedimentation rates and radiative transfer (Kärcher et al., 2023). The use of constant deposition coefficients may therefore cause biases in AIC lifetime predictions regardless of the computational method employed. This means that in the absence of low temperature growth measurements of individual crystals, we lack important information that can be used to constrain AIC lifetime statistics. Intercomparison exercises between high-fidelity AIC models in conjunction with improved observational strategies capturing the stabilization regime are needed to improve this situation.

An advantage of the present model is that it allows us to implement the stochastic forcing of contrail evolution by internal gravity waves and to generate AIC lifetime statistics based on thousands of individual simulations. Large-eddy simulations allow the impact of aircraft wake evolution, atmospheric turbulence, or wind shear on contrail evolution to be studied realistically (Lewellen et al., 2014; Naiman et al., 2011; Paoli et al., 2013; Paugam et al., 2010; Unterstrasser, 2014). Regional- or cloud-scale models with comprehensive cirrus microphysics, online radiative transfer, and realistic dynamical boundary conditions are needed to investigate AIC across the whole lifespan, including effects of contrail radiative heating.

KÄRCHER AND CORCOS 20 of 28

Deep convection is the main source of gravity waves in the tropics. Observations show that tropical gravity wave amplitude and frequency composition depend on the distance from deep convective sources. Other sources, more important at midlatitudes where contrails are more abundant, include heterogeneous orography, mountains, thunderstorms, and atmospheric jets and fronts (Nappo, 2013; Plougonven & Zhang, 2014). Gravity wave intermittency is related to their sources, and although convective cells are highly intermittent, the ubiquity of convection in the tropical band lowers the overall level of intermittency compared to higher latitudes, as shown by observations (Corcos et al., 2021; Hertzog et al., 2012; Wright et al., 2013). This aspect of intermittency is not accounted for in our study, but is required to force AIC evolution realistically. Another source of uncertainty in the applied wave forcing is related to the possible enhancement of vertical wind speed variance near the Brunt-Väisälä frequency attributed to trapped gravity waves (Kottayil et al., 2025).

We finally point to a structural deficiency of all AIC plume models. Persistent contrails may form inside preexisting cirrus clouds (Tesche et al., 2016; Verma & Burkhardt, 2022) or cirrus may form in air surrounding persistent contrails. An example of the latter would be the ice nucleation pathway addressed here. Since AIC plume models simulate individual contrails forming and evolving in otherwise cloud-free air, they do not account for perturbations of, or interactions with, natural cirrus clouds. In addition, we note that the interaction of contrailprocessed soot aerosol with natural cirrus (Kärcher et al., 2021) affects the very definition of AIC. Clearly, addressing these issues is important for the evaluation of AIC mitigation options.

5.4. Implications for Future Work

Uncertainty in the prediction of ice-supersaturated regions is commonly regarded as the largest uncertainty in quantifying global AIC RF (Lee et al., 2023). The present study suggests that limited observations of AIC lifetimes and associated poor skill of AIC models adds significant further uncertainty.

The conceptualization and analysis of AIC lifetime statistics presented here aids satellite analyses. For example, it would be highly useful to stratify estimates of AIC lifetimes according to ice supersaturation and gravity wave activity in a given synoptic situation (large-scale warming or cooling). This might lead to improved contrail parameterizations and models that rely less on tuning. In this regard, applications of our model framework may benefit from a more realistic representation of synoptic variations, including Lagrangian temporal variations and constraints on the magnitude of key parameters (e.g., vertical wind speed fluctuations, and ice supersaturation) in such situations.

As initial contrail properties are strongly fuel-dependent (Yu et al., 2024) and aviation fuel effects on AIC lifetimes have not been thoroughly studied experimentally, substantial uncertainty exists regarding the role of alternative aviation fuels in mitigating AIC RF. Our study suggests that initializing contrail models with a proper representation of the ice crystal size distribution is particularly relevant to simulate lifetimes of AIC produced by alternative aviation fuels. in situ measurements and process models find an increase in initial mean ice crystal size relative to contrails produced by kerosene combustion (Voigt et al., 2021; Yu et al., 2024). It is recommended that models that vary initial ice number concentrations to assess fuel effects on contrail evolution discuss associated changes in initial ice crystal sizes in relation to observational evidence and the model representation of dynamical forcing. We suggest comparing simulated ice crystal size distributions to measurements taken in the vortex-dissipation regime of aircraft wake development.

Past studies addressed changes in surface shortwave radiation due to cirrus clouds, an interesting area of research that received little attention in the aviation community. Lidar measurements near Paris, France, revealed that almost half of the situations classified by analysis of irradiance measurements as cloudless sky periods were actually characterized by the presence of ice water in high, subvisible or semi-transparent cirrus clouds (Dupont et al., 2008). Broadband shortwave radiation increased at several locations across the continental USA in the decade 1996–2007 and the observed trend was almost entirely due to increased diffuse radiance (clear-sky whitening) (Long et al., 2009). The authors of the latter study hypothesized that an increase in optically thin, contrail-generated ice crystal haze explains this phenomenon (Kärcher, 2018).

Our analysis of AIC lifetimes as summarized in Figure 7, with particular emphasis on the stabilization regime, supports a possible role of aviation in clear-sky whitening. Long-lived contrails are mostly optically thin and associated with large horizontal coverage when allowed to accumulate over a day in areas with dense air traffic (Burkhardt & Kärcher, 2009). Arguably, the above radiation measurements provide a unique opportunity to put

KÄRCHER AND CORCOS 21 of 28

AIC models, including their radiative transfer parameterizations, under scientific scrutiny. Combining active and passive remote sensing with in situ measurements and regional (high resolution) modeling of AIC helps reduce uncertainty in predictions of AIC microphysical properties and RF.

Reliable prediction of persistent contrails and contrail cirrus is only one but a fundamental element in assessing the climate impact of AIC. The apparent dearth of rigorous AIC model evaluation and validation at the process level implies that current knowledge on the AIC lifecycle is incomplete. The resulting lack of confidence in AIC model predictions hampers climate impact mitigation via contrail avoidance. By addressing how fundamental cloud processes driven by meteorological variability impact AIC lifetimes, our study reveals room for improving the physical basis of AIC parameterizations and models. Pending scientific knowledge gaps need to be closed—in particular regarding microphysical properties and radiative significance of AIC in the stabilization regime and contrail-perturbed natural cirrus cloudiness—in order to make AIC mitigation strategies practicable. This goal may be best achieved within a targeted research program allying field and laboratory experiments with numerical cloud, radiation, and climate modeling across a range of scales.

Appendix A: Evolution of Contrail Ice Crystal Size Distributions

We report the evolution of a contrail ice crystal size distribution for one statistical realization of baseline scenario GW ($\bar{w} = 0.15 \text{ m s}^{-1}$, $s_a = 0$, L = 1 km). The example shown in Figure A1 illustrates one case with a lifetime of 10.5 hr; recall the mean lifetime of 2.64 hr in this scenario (Table 2). This example illustrates a contrail's lifecycle that is ended by sedimentation. For convenience, we repeat the initial distribution from Figure 4 along with distributions picked at contrail ages within the three evolutionary regimes discussed in Section 5.

The initial size distribution is given by a Gamma distribution with a mean radius of $1.5\,\mu m$ in line with Kleine et al. (2018). The total ice crystal number concentration decreases continuously due to plume dilution. The distribution shifts to a mean radius near $4\,\mu m$ in the adjustment regime and is left skewed due to active sublimation losses, in line with in situ measurements (Schröder et al., 2000). We refer to Section 4.1 for a more detailed discussion of underlying processes.

A few hours later in the stabilization regime, the distribution attains a relatively stable mean radius short of $10 \,\mu\text{m}$. Although sublimation is still active as indicated by the left-skewed distribution, gravity wave-driven sublimation events do not induce significant ice crystal losses. Moreover, ice crystals larger than $15-20 \,\mu\text{m}$ in radius, produced during wave-driven growth events, settle out of the ice-supersaturated layer. We point out

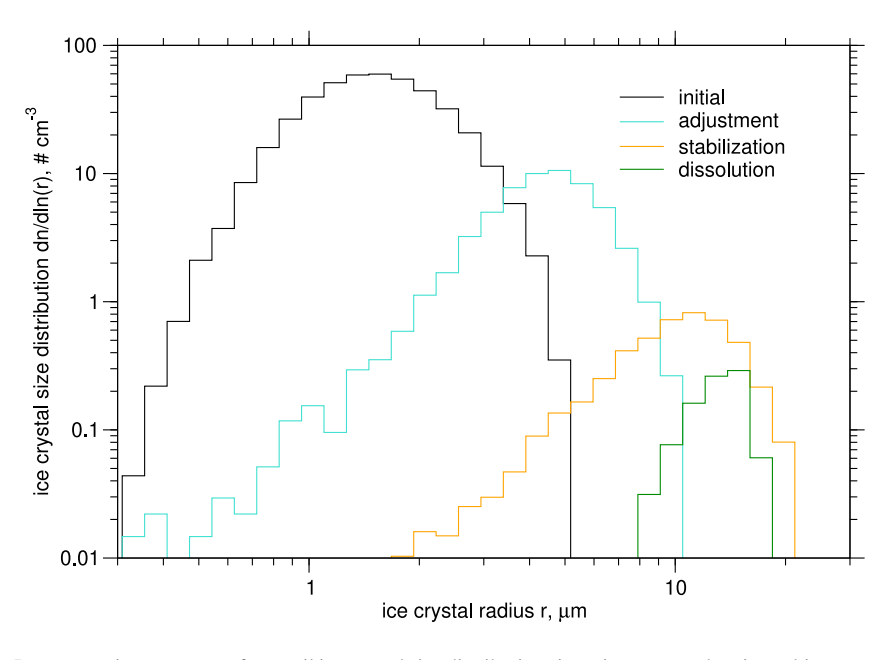


Figure A1. Representative sequence of contrail ice crystal size distributions in an ice-saturated region subject to gravity wave activity.

KÄRCHER AND CORCOS 22 of 28



that the predicted mean ice crystal size is in line with in situ measurements in a contrail cirrus outbreak (Wang et al., 2023), underscoring the realism of our simulations. Toward the end of this contrail's lifetime, the significantly narrowed size distribution covers the $8-16\,\mu m$ radius range before the last remaining ice crystals leave the contrail layer.

Glossary

0	initial
a	ambient (air)
c	contrail
f	(supersaturation) forcing
gw	gravity wave
1	(contrail) lifetime
min	minimum
med	median
max	maximum
n	(ice) nucleation
q	(ice supersaturation) quenching
S	synoptic
sat	ice saturation
t	turbulent
v	(water) vapor
-	mean value (Laplacian: mean absolute deviation)
•	wave amplitude (peak value)
.′	fluctuation
i	index counting time steps
j	index counting simulation ice particles $(j = 1,, J)$
b	entrainment rate power law index
f	Coriolis (inertial) frequency
g	acceleration due to gravity
l	buoyancy length scale
ℓ	diffusion length scale for water molecules in air
n	total ice crystal number concentration
p	air pressure
q	mass mixing ratio
r	ice crystal radius
S	ice supersaturation
t	time; contrail age
w	total vertical wind speed

KÄRCHER AND CORCOS 23 of 28

Z	altitude
C	Cunningham slip correction factor for terminal fall speeds
\mathcal{C}	correlation coefficient for turbulent fluctuations
\mathcal{D}	dilution factor per time step
D	effective diffusion coefficient for H ₂ O in air
J	total (initial) number of simulation ice particles
H	latent heat of sublimation
L	ice-supersaturated layer depth including the contrail
N	Brunt-Väisälä (buoyancy) frequency
P	probability of ice nucleation if <1
$dP/d \ln r$	initial ice crystal number-size (probability) distribution
Q	Mie extinction (scattering) efficiency
R	ice nucleation rate per unit length of updraft
\mathcal{R}	specific gas constant
$\mathcal S$	ice supersaturation over an ice crystal surface
T	air temperature
V	ice crystal terminal fall speed
Z	altitude of ice crystals relative to lower contrail boundary
α	deposition coefficient for uptake of H ₂ O on ice crystals
β	contrail extinction
γ	lapse rate in air surrounding the contrail
Γ	dry adiabatic lapse rate
δt	model time step
δz	contrail vertical depth
η	ice crystal number mixing ratio per unit mass of air
κ	factor converting temperature into cloud-free supersaturation fluctuations
μ	shape parameter of Gamma size distribution
ν	dynamic viscosity of air
ω	entrainment rate; wave frequency
g	mass density of air
φ	wave phase
σ	standard deviation
τ	shortwave contrail column optical depth
Ψ	Laplacian (double-sided exponential) random variate
ξ	Gaussian random variate (zero mean, unit variance)
ζ	random variate uniformly distributed within [0,1]

KÄRCHER AND CORCOS 24 of 28

Acknowledgments

We gratefully acknowledge fruitful

discussions with David Lee and Michael

Ponater. M.C. received funding from the

National Science Foundation under Grant

2231667. Open Access funding enabled

and organized by Projekt DEAL.

Journal of Geophysical Research: Atmospheres

Acronyms

ACTA automatic contrail tracking algorithm

AIC aircraft-induced cloudiness

CO₂ carbon dioxide

H₂O water molecules in air (water vapor)

PDF probability density function

RF radiative forcing

SIP simulation ice particle

Conflict of Interest

The authors declare no conflict of interest relevant to this study.

Data Availability Statement

Simulated data produced in this study are publicly available (Kärcher & Corcos, 2025).

References

Abade, G. C., Grabowski, W. W., & Pawlowska, H. (2018). Broadening of cloud droplet spectra through eddy hopping: Turbulent entraining parcel simulations. *Journal of the Atmospheric Sciences*, 75(10), 3365–3379. https://doi.org/10.1175/JAS-D-18-0078.1

Bakan, S., Betancor, M., Gayler, V., & Grassl, H. (1994). Contrail frequency over Europe from NOAA-satellite images. *Annales Geophysicae*, 12(10/11), 962–968. https://doi.org/10.1007/s00585-994-0962-y

Bartosch, L. (2001). Generation of colored noise. International Journal of Modern Physics C, 12(6), 851–855. https://doi.org/10.1142/S0129183101002012

Becken, S., & Mackey, B. (2017). What role for offsetting aviation greenhouse gas emissions in a deep-cut carbon world. *Journal of Air Transport Management*, 63, 71–83. https://doi.org/10.1016/j.jairtraman.2017.05.009

Bickel, M., Ponater, M., Bock, L., Burkhardt, U., & Reineke, S. (2020). Estimating the effective radiative forcing of contrail cirrus. *Journal of Climate*, 33(5), 1991–2005. https://doi.org/10.1175/JCLI-D-19-0467.1

Bickel, M., Ponater, M., Burkhardt, U., Righi, M., Hendricks, J., & Jöckel, P. (2025). Contrail cirrus climate impact: From radiative forcing to surface temperature change. *Journal of Climate*, 38(8), 1895–1912. https://doi.org/10.1175/JCLI-D-24-0245.1

Bock, L., & Burkhardt, U. (2016). The temporal evolution of a long-lived contrail cirrus cluster: Simulations with a global climate model. *Journal of Geophysical Research: Atmospheres*, 121(7), 3548–3565. https://doi.org/10.1002/2015JD024475

Borella, A., Boucher, O., Shine, K. P., Stettler, M., Tanaka, K., Teoh, R., & Bellouin, N. (2024). The importance of an informed choice of CO₂-equivalence metrics for contrail avoidance. *Atmospheric Chemistry and Physics*, 24(16), 9401–9417. https://doi.org/10.5194/acp-24-9401-2024

Brazzola, N., Patt, A., & Wohland, J. (2022). Definitions and implications of climate-neutral aviation. *Nature Climate Change*, 12(8), 761–767. https://doi.org/10.1038/s41558-022-01404-7

Burkhardt, U., Bock, L., & Bier, A. (2018). Mitigating the contrail cirrus climate impact by reducing aircraft soot number emissions. npj Climate and Atmospheric Science, 1, 37. https://doi.org/10.1038/s41612-018-0046-4

Burkhardt, U., & Kärcher, B. (2009). Process-based simulation of contrail cirrus in a global climate model. *Journal of Geophysical Research*, 114(D16). https://doi.org/10.1029/2008JD011491

Burkhardt, U., & Kärcher, B. (2011). Global radiative forcing from contrail cirrus. *Nature Climate Change*, 1, 54–58. https://doi.org/10.1038/nclimate1068

Burkhardt, U., Kärcher, B., Ponater, M., Gierens, K., & Gettelman, A. (2008). Contrail cirrus supporting areas in model and observations. Geophysical Research Letters, 35(16). https://doi.org/10.1029/2008GL034056

Caiazzo, F., Agarwal, A., Speth, R. L., & Barrett, S. R. H. (2017). Impact of biofuels on contrail warming. Environmental Research Letters, 12(11), 114013. https://doi.org/10.1088/1748-9326/aa893b

Callies, J., Ferrari, R., & Bühler, O. (2014). Transition from geostrophic turbulence to inertia-gravity waves in the atmospheric energy spectrum. Proceedings of the National Academy of Sciences of the United States of America, 111(48), 17033–17038. https://doi.org/10.1073/pnas. 1410772111

Chen, C.-C., & Gettelman, A. (2013). Simulated radiative forcing from contrails and contrail cirrus. Atmospheric Chemistry and Physics, 13(24), 12525–12536. https://doi.org/10.5194/acp-13-12525-2013

Corcos, M., Hertzog, A., Plougonven, R., & Podglajen, A. (2021). Observation of gravity waves at the tropical tropopause using superpressure balloons. *Journal of Geophysical Research: Atmospheres*, 126(15), e2021JD035165. https://doi.org/10.1029/2021JD035165

Diao, M., Zondlo, M. A., Heymsfield, A. J., Avallone, L. M., Paige, M. E., Beaton, S. P., et al. (2014). Cloud-scale ice-supersaturated regions spatially correlate with high water vapor heterogeneities. *Atmospheric Chemistry and Physics*, 14(5), 2639–2656. https://doi.org/10.5194/acp-14-2639-2014

Driver, O. G. A., Stettler, M. E. J., & Gryspeerdt, E. (2025). Synoptic and microphysical lifetime constraints for contrails. Atmospheric Measurement Techniques, 18(5), 1115–1134. https://doi.org/10.5194/amt-18-1115-2025

Dupont, J.-C., Haeffelin, M., & Long, C. N. (2008). Evaluation of cloudless-sky periods detected by shortwave and longwave algorithms using lidar measurements. *Geophysical Research Letters*, 35(10). https://doi.org/10.1029/2008GL033658

KÄRCHER AND CORCOS 25 of 28

- Dürbeck, T., & Gerz, T. (1996). Dispersion of aircraft exhausts in the free atmosphere. *Journal of Geophysical Research*, 101(D20), 26007–26015. https://doi.org/10.1029/96JD02217
- Fahey, D. W., & Schumann, U. (1999). Aviation-produced aerosols and cloudiness. Aviation and the global atmosphere. A special report of IPCC working groups I and III. Intergovernmental panel on climate change special report. Retrieved from https://www.ipcc.ch/report/aviation-and-the-global-atmosphere-2
- Forster, P., Storelvmo, T., Armour, K., Collins, W., Dufresne, J.-L., Frame, D., et al. (2021). The Earth's energy budget, climate feedbacks, and climate sensitivity. Climate change 2021: The physical science basis. Contribution of working group I to the sixth assessment report of the intergovernmental panel on climate change. Retrieved from www.ipcc.ch/report/ar6/wg1/downloads/report/IPCC_AR6_WGI_Chapter07.pdf
 Fritts, D. C., & Alexander, M. J. (2003). Gravity wave dynamics and effects in the middle atmosphere. Review of Geophysics, 41(1), https://doi.
- org/10.1029/2001RG000106
- Fritz, T. M., Eastham, S. D., Speth, R. L., & Barrett, S. R. H. (2020). The role of plume-scale processes in long-term impacts of aircraft emissions. Atmospheric Chemistry and Physics, 20(9), 5697–5727. https://doi.org/10.5194/acp-20-5697-2020
- Gettelman, A., Fetzer, E. J., Eldering, A., & Irion, F. W. (2006). The global distribution of supersaturation in the upper troposphere from the atmospheric infrared sounder. *Journal of Climate*, 19(23), 6089–6103. https://doi.org/10.1175/JCLI3955.1
- Gierens, K., Matthes, S., & Rohs, S. (2020). How well can persistent contrails be predicted? Aerospace, 7(12), 169. https://doi.org/10.3390/aerospace7120169
- Gierens, K., Schumann, U., Helten, M., Smit, H., & Marenco, A. (1999). A distribution law for relative humidity in the upper troposphere and lower stratosphere derived from three years of MOZAIC measurements. *Annales Geophysicae*, 17(9), 1218–1226. https://doi.org/10.1007/s00585-999-1218-7
- Gierens, K., & Vazquez-Navarro, M. (2018). Statistical analysis of contrail lifetimes from a satellite perspective. *Meteorologische Zeitschrift*, 27. https://doi.org/10.1127/metz/2018/0888
- Grewe, V., Rao, A. G., Grönstedt, T., Xisto, C., Linke, F., Melkert, J., et al. (2021). Evaluating the climate impact of aviation emission scenarios towards the Paris agreement including COVID-19 effects. *Nature Communications*, 12(1), 3841. https://doi.org/10.1038/s41467-021-24091-y
- Gryspeerdt, E., Stettler, M., Teoh, R., Burkhardt, U., Delovski, T., Driver, O., & Painemal, D. (2024). Operational differences lead to longer lifetimes of satellite detectable contrails from more fuel efficient aircraft. *Environmental Research Letters*, 19(8), 084059. https://doi.org/10.1088/1748-9326/ad5b78
- Haywood, J. M., Allan, R. P., Bornemann, J., Forster, P. M., Francis, P. N., Milton, S., et al. (2009). A case study of the radiative forcing of persistent contrails evolving into contrail-induced cirrus. *Journal of Geophysical Research*, 114(D24). https://doi.org/10.1029/2009JD012650
- Hertzog, A., Alexander, M. J., & Plougonven, R. (2012). On the intermittency of gravity wave momentum flux in the stratosphere. *Journal of the Atmospheric Sciences*, 69(11), 3433–3448. https://doi.org/10.1175/JAS-D-12-09.1
- Hofer, S. M., & Gierens, K. M. (2025). Synoptic and microphysical lifetime constraints for contrails. Atmospheric Chemistry and Physics Discussions, 25. https://doi.org/10.5194/egusphere-2025-326
- Irvine, E. A., Hoskins, B. J., & Shine, K. P. (2014). Lagrangian analysis of ice-supersaturated air over the North Atlantic. *Journal of Geophysical Research: Atmospheres*, 119(1), 90–100. https://doi.org/10.1002/2013JD020251
- Iwabuchi, H., Yang, P., Liou, K. N., & Minnis, P. (2012). Physical and optical properties of persistent contrails: Climatology and interpretation. Journal of Geophysical Research, 117(D6). https://doi.org/10.1029/2011JD017020
- Jensen, E. J., Kärcher, B., Woods, S., Krämer, M., & Ueyama, R. (2024). The impact of gravity waves on the evolution of tropical anvil cirrus microphysical properties. *Journal of Geophysical Research: Atmospheres*, 129(5), e2023JD039887. https://doi.org/10.1029/2023JD039887
- Kärcher, B. (2005). Supersaturation, dehydration, and denitrification in Arctic cirrus. Atmospheric Chemistry and Physics, 5(7), 1757–1772. https://doi.org/10.5194/acp-5-1757-2005
- Kärcher, B. (2018). Formation and radiative forcing of contrail cirrus. *Nature Communications*, 9(1), 1824. https://doi.org/10.1038/s41467-018-04068-0
- Kärcher, B., Burkhardt, U., Bier, A., Bock, L., & Ford, I. J. (2015). The microphysical pathway to contrail formation. *Journal of Geophysical Research: Atmospheres*, 120(15), 7893–7927. https://doi.org/10.1002/2015JD023491
- Kärcher, B., Burkhardt, U., Ponater, M., & Frömming, C. (2010). Importance of representing optical depth variability for estimates of global line-shaped contrail radiative forcing. Proceedings of the National Academy of Sciences of the United States of America, 107(45), 19181–19184. https://doi.org/10.1073/pnas.1005555107
- Kärcher, B., Burkhardt, U., Unterstrasser, S., & Minnis, P. (2009). Factors controlling contrail cirrus optical depth. Atmospheric Chemistry and Physics, 9(16), 6229–6254. https://doi.org/10.5194/acp-9-6229-2009
- Kärcher, B., & Corcos, M. (2025). On the lifetimes of persistent contrails and contrail cirrus [Dataset]. Zenodo. https://doi.org/10.5281/zenodo. 17199620
- Kärcher, B., DeMott, P. J., Jensen, E. J., & Harrington, J. Y. (2022). Studies on the competition between homogeneous and heterogeneous ice nucleation in cirrus formation. *Journal of Geophysical Research: Atmospheres*, 127. https://doi.org/10.1029/2022JD035805
- Kärcher, B., Hoffmann, F., Podglajen, A., Hertzog, A., Plougonven, R., Atlas, R., et al. (2024). Effects of turbulence on upper-tropospheric ice supersaturation. *Journal of the Atmospheric Sciences*, 81(9), 1589–1604. https://doi.org/10.1175/JAS-D-23-0217.1
- Kärcher, B., Hoffmann, F., Sokol, A. B., Gasparini, B., Corcos, M., Jensen, E., et al. (2025). Dissecting cirrus clouds: Navigating effects of turbulence on homogeneous ice formation. npj Climate and Atmospheric Science, 8(1), 137. https://doi.org/10.1038/s41612-025-01024-w
- Kärcher, B., Jensen, E. J., Pokrifka, G. F., & Harrington, J. Y. (2023). Ice supersaturation variability in cirrus clouds: Role of vertical wind speeds and deposition coefficients. *Journal of Geophysical Research: Atmospheres*, 128(22), e2023JD039324. https://doi.org/10.1029/2023JD039324
- Kärcher, B., Mahrt, F., & Marcolli, C. (2021). Process-oriented analysis of aircraft soot-cirrus interactions constrains the climate impact of aviation. *Communications Earth & Environment*, 2(1), 113. https://doi.org/10.1038/s43247-021-00175-x
- Kärcher, B., & Podglajen, A. (2019). A stochastic representation of temperature fluctuations induced by mesoscale gravity waves. *Journal of Geophysical Research: Atmospheres*, 124(21), 11506–11529. https://doi.org/10.1029/2019JD030680
- Kleine, J., Voigt, C., Sauer, D., Schlager, H., Scheibe, M., Jurkat-Witschas, T., et al. (2018). In situ observations of ice particle losses in a young persistent contrail. *Geophysical Research Letters*, 45(24). https://doi.org/10.1029/2018GL079390
- Klöwer, M., Allen, M. R., Lee, D. S., Proud, S. R., Gallagher, L., & Skowron, A. (2021). Quantifying aviation's contribution to global warming. Environmental Research Letters, 16(10), 104027. https://doi.org/10.1088/1748-9326/ac286e
- Köhler, L., Green, B., & Stephan, C. C. (2023). Comparing loon superpressure balloon observations of gravity waves in the tropics with global storm-resolving models. *Journal of Geophysical Research: Atmospheres*, 128(15), e2023JD038549. https://doi.org/10.1029/2023JD038549
- Korolev, A. V., & Mazin, I. P. (2003). Supersaturation of water vapor in clouds. *Journal of the Atmospheric Sciences*, 60(2). https://doi.org/10.1175/1520-0469(2003)060<3C2957:SOWVIC>2.0.CO;2

KÄRCHER AND CORCOS 26 of 28

- Kottayil, A., Podglajen, A., Legras, B., Atlas, R., Prajwal, K., Satheesan, K., & Abhilash, S. (2025). High-frequency gravity waves and Kelvin-Helmholtz billows in the tropical UTLS, as seen from radar observations of vertical wind. *Geophysical Research Letters*, 51(21), e2024GL110366. https://doi.org/10.1029/2024GL110366
- Lamb, D., & Verlinde, J. (2011). Physics and chemistry of clouds. University Press.
- Lamquin, N. J. C., Stubenrauch, Gierens, K., Burkhardt, U., & Smit, H. (2012). A global climatology of upper-tropospheric ice supersaturation occurrence inferred from the atmospheric infrared sounder calibrated by MOZAIC. Atmospheric Chemistry and Physics, 12(1), 381–405. https://doi.org/10.5194/acp-12-381-2012
- Lee, D. S., Allen, M. R., Cumpsty, N., Owen, B., Shine, K. P., & Skowron, A. (2023). Uncertainties in mitigating aviation non-CO₂ emissions for climate and air quality using hydrocarbon fuels. *Environmental Science: Atmosphere*, 3(12), 1693–1740. https://doi.org/10.1039/d3ea00091e
- Lee, D. S., Fahey, D. W., Skowron, A., Allen, M. R., Burkhardt, U., Chen, Q., et al. (2021). The contribution of global aviation to anthropogenic climate forcing for 2000 to 2018. Atmospheric Environment, 244, 117834. https://doi.org/10.1016/j.atmosenv.2020.117834
- Lewellen, D. C., Meza, O., & Huebsch, W. W. (2014). Persistent contrails and contrail cirrus. Part I: Large-eddy simulations from inception to demise. *Journal of the Atmospheric Sciences*, 71(12), 4399–4419. https://doi.org/10.1175/JAS-D-13-0316.1
- Lin, R.-F., Starr, D. O., Reichardt, J., & DeMott, P. J. (2005). Nucleation in synoptically forced cirrostratus. *Journal of Geophysical Research*, 110(D8). https://doi.org/10.1029/2004JD005362
- Lohmann, U., Spichtinger, P., Jess, S., Peter, T., & Smit, H. (2008). Cirrus cloud formation and ice supersaturated regions in a global climate
- model. Environmental Research Letters, 3(4), 045022. https://doi.org/10.1088/1748-9326/3/4/045022 Long, C. N., Dutton, E. G., Augustine, J. A., Wiscombe, W., Wild, M., McFarlane, S. A., & Flynn, C. J. (2009). Significant decadal brightening of
- downwelling shortwave in the continental United States. *Journal of Geophysical Research*, 114(D10). https://doi.org/10.1029/2008JD011263 Magee, N. B., Miller, A., Amaral, M., & Cumiskey, A. (2014). Mesoscopic surface roughness of ice crystals pervasive across a wide range of ice
- crystal conditions. Atmospheric Chemistry and Physics, 14(22), 12357–12371. https://doi.org/10.5194/acp-14-12357-2014

 Martinez, C. A., Eastham, S. D., & Jarrett, J. P. (2025). Contrail models lacking post-fallstreak behavior could underpredict lifetime optical depth.

 Atmospheric Chemistry and Physics Discussions, 25. https://doi.org/10.5194/egusphere-2025-278
- Miloshevich, L. M., & Heymsfield, A. J. (1997). A balloon-borne continuous cloud particle replicator for measuring vertical profiles of cloud microphysical properties: Instrument design, performance, and collection efficiency analysis. *Journal of Atmospheric and Oceanic Technology*, 14, https://doi.org/10.1175/1520-0426(1997)014.0753;ABBCCP.2.0.CO:2
- Minnis, P. (2003). Contrails. In J. Holton, J. Pyle, & J. Curry (Eds.), Encyclopedia of atmospheric sciences. Academic Press.
- Minnis, P., Young, D. F., Garber, D. P., Nguyen, L., Jr., & Palikonda, R. (1998). Transformation of contrails into cirrus during SUCCESS. Geophysical Research Letters, 25(8), 1157–1160. https://doi.org/10.1029/97GL03314
- Naiman, A. D., Lele, S. K., & Jacobsen, M. Z. (2011). Large eddy simulations of contrail development: Sensitivity to initial and ambient conditions over first twenty minutes. *Journal of Geophysical Research*, 116(D21), https://doi.org/10.1029/2011JD015806
- Nappo, C. J. (2013). An introduction to atmospheric gravity waves. Elsevier.

org/10.1029/2005GL022580

- Newinger, C., & Burkhardt, U. (2012). Sensitivity of contrail cirrus radiative forcing to air traffic scheduling. *Journal of Geophysical Research*, 117(D10). https://doi.org/10.1029/2011JD016736
- Paoli, R., Nybelen, L., Picot, J., & Cariolle, D. (2013). Effects of jet/vortex interaction on contrail formation in supersaturated conditions. *Physics of Fluids*, 25(5), 053305. https://doi.org/10.1063/1.4807063
- Paoli, R., & Shariff, K. (2016). Contrail modeling and simulation. Annual Review of Fluid Mechanics, 48(1), 393–427. https://doi.org/10.1146/annurev-fluid-010814-013619
- Paugam, R., Paoli, R., & Cariolle, D. (2010). Influence of vortex dynamics and atmospheric turbulence on the early evolution of a contrail. Atmospheric Chemistry and Physics, 10(8), 3933–3952. https://doi.org/10.5194/acp-10-3933-2010
- Petzold, A., Neis, P., Rütimann, M., Rohs, S., Berkes, F., Smit, H. G. J., et al. (2020). Ice-supersaturated air masses in the northern mid-latitudes from regular in situ observations by passenger aircraft: Vertical distribution, seasonality and tropospheric fingerprint. *Atmospheric Chemistry and Physics*, 20(13), 8157–8179. https://doi.org/10.5194/acp-20-8157-2020
- Plougonven, R., & Zhang, F. (2014). Internal gravity waves from atmospheric jets and fronts. Review of Geophysics, 52(1), 33–76. https://doi.org/10.1002/2012RG000419
- Podglajen, A., Hertzog, A., Plougonven, R., & Legras, B. (2016). Lagrangian temperature and vertical velocity fluctuations due to gravity waves in the lower stratosphere. Geophysical Research Letters, 43(7), 3543–3553. https://doi.org/10.1002/2016GL068148
- Podglajen, A., Hertzog, A., Plougonven, R., & Legras, B. (2020). Lagrangian gravity wave spectra in the lower stratosphere of current (re)analyses. Atmospheric Chemistry and Physics, 20(15), 9331–9350. https://doi.org/10.5194/acp-20-9331-2020
- Polichtchouk, I., Wedi, N., & Kim, Y.-H. (2021). Resolved gravity waves in the tropical stratosphere: Impact of horizontal resolution and deep convection parametrization. *The Quarterly Journal of the Royal Meteorological Society, 148*(742), 233–251. https://doi.org/10.1002/qj.4202
 Ponater, M., Marquart, S., Sausen, R., & Schumann, U. (2005). On contrail climate sensitivity. *Geophysical Research Letters, 32*(10). https://doi.
- Ramaswamy, V., Collins, W., Haywood, J., Lean, J., Mahowald, N., Myhre, G., et al. (2019). Radiative forcing of climate: The historical evolution of the radiative forcing concept, the forcing agents and their quantification, and applications. *Meteorological Monographs*, 59, 14.1–14.101. https://doi.org/10.1175/AMSMONOGRAPHS-D-19-0001.1
- Rap, A., Forster, P. M., Haywood, J. M., Jones, A., & Boucher, O. (2010). Estimating the climate impact of linear contrails using the UK Met Office climate model. *Geophysical Research Letters*, 37(20). https://doi.org/10.1029/2010GL045161
- Reutter, P., Neis, P., Rohs, S., & Sauvage, B. (2020). Ice supersaturated regions: Properties and validation of ERA-interim reanalysis with IAGOS in situ water vapour measurements. Atmospheric Chemistry and Physics, 20(2), 787–804. https://doi.org/10.5194/acp-20-787-2020
- Rui, D., Pokrifka, G. F., Moyle, A. M., & Harrington, J. Y. (2025). The growth of ice crystals formed from frozen solution droplets: Laboratory measurements and power-law parameterization. *Journal of the Atmospheric Sciences*, 82(4), 775–788. https://doi.org/10.1175/JAS-D-24-0182.1
- Schröder, F., Kärcher, B., Duroure, C., Ström, J., Petzold, A., Gayet, J.-F., et al. (2000). On the transition of contrails into cirrus clouds. *Journal of the Atmospheric Sciences*, 57(4), 464–480. https://doi.org/10.1175/1520-0469(2000)057<0464:ottoci>2.0.co;2
- Schumann, U. (2012). A contrail cirrus prediction model. Geoscientific Model Development, 5(3), 543–580. https://doi.org/10.5194/gmd-5-543-2012
- Schumann, U., Schlager, H., Arnold, F., Baumann, R., Haschberger, P., & Klemm, O. (1998). Dilution of aircraft exhaust plumes at cruise altitudes. *Atmospheric Environment*, 32(18), 3097–3103. https://doi.org/10.1016/S1352-2310(97)00455-X
- Sölch, I., & Kärcher, B. (2010). A large-eddy model for cirrus clouds with explicit aerosol and ice microphysics and Lagrangian ice particle tracking. The Quarterly Journal of the Royal Meteorological Society, 136(653), 2074–2093. https://doi.org/10.1002/qj.689

KÄRCHER AND CORCOS 27 of 28

- Spichtinger, P., Gierens, K., & Dörnbrack, A. (2005). Formation of ice supersaturation by mesoscale gravity waves. *Atmospheric Chemistry and Physics*, 5, 1243–1255. https://doi.org/10.5194/acp-5-1243-2005
- Spichtinger, P., Gierens, K., & Read, W. (2003). The global distribution of ice-supersaturated regions as seen by the Microwave Limb Sounder. The Quarterly Journal of the Royal Meteorological Society, 129(595), 3391–3410. https://doi.org/10.1256/qj.02.141
- Stuber, N., Forster, P., R\u00e4del, G., & Shine, K. (2006). The importance of the diurnal and annual cycle of air traffic for contrail radiative forcing. Nature, 441(7095), 864–867. https://doi.org/10.1038/nature04877
- Teoh, R., Schumann, U., Majumdar, A., & Stettler, M. E. J. (2020). Mitigating the climate forcing of aircraft contrails by small-scale diversions and technology adoption. *Environmental Research & Technology*, 54(5), 2941–2950. https://doi.org/10.1021/acs.est.9b05608
- Tesche, M., Achtert, P., Glantz, P., & Noone, K. J. (2016). Aviation effects on already-existing cirrus clouds. *Nature Communications*, 7(1), 12016. https://doi.org/10.1038/ncomms12016
- Unterstrasser, S. (2014). Large-eddy simulation study of contrail microphysics and geometry during the vortex phase and consequences on contrail-to-cirrus transition. *Journal of Geophysical Research: Atmospheres*, 119(12), 7537–7555. https://doi.org/10.1002/2013JD021418 van de Hulst, H. C. (1981). *Light scattering by small particles*. Dover Publication.
- Vazquez-Navarro, M., Mannstein, H., & Kox, S. (2015). Contrail life cycle and properties from 1 year of MSG/SEVIRI rapid-scan images. Atmospheric Chemistry and Physics, 15, 8739–8749. https://doi.org/10.5194/acp-15-8739-2015
- Verma, P., & Burkhardt, U. (2022). Contrail formation within cirrus: ICON-LEM simulations of the impact of cirrus cloud properties on contrail formation. *Atmospheric Chemistry and Physics*, 22(13), 8819–8842. https://doi.org/10.5194/acp-22-8819-2022
- Voigt, C., Kleine, J., Sauer, D., Moore, R. H., Bräuer, T., LeClercq, P., et al. (2021). Cleaner burning aviation fuels can reduce contrail cloudiness. Communications Earth & Environment, 2(1), 114. https://doi.org/10.1038/s43247-021-00174-y
- Voigt, C., Schumann, U., Jessberger, P., Jurkat, T., Petzold, A., Gayet, J.-F., et al. (2011). Extinction and optical depth of contrails. Geophysical Research Letters, 38(11). https://doi.org/10.1029/2011GL047189
- Wang, Z., Bugliaro, L., Jurkat-Witschas, T., Heller, R., Burkhardt, U., Ziereis, H., et al. (2023). Observations of microphysical properties and radiative effects of a contrail cirrus outbreak over the North Atlantic. *Atmospheric Chemistry and Physics*, 23(3), 1941–1961. https://doi.org/10.5194/acp-23-1941-2023
- Warhaft, Z. (2000). Passive scalars in turbulent flows. Annual Review of Fluid Mechanics, 32(1), 203–240. https://doi.org/10.1146/annurev.fluid.
- Wilhelm, L., Gierens, K., & Rohs, S. (2022). Meteorological conditions that promote persistent contrails. Applied Sciences, 12(9), 4450. https://doi.org/10.3390/app12094450
- WMO, W. M. O. (2017). Cloud atlas. Retrieved from https://cloudatlas.wmo.int/aircraft-condensation-trails.html
- Wolf, K., Bellouin, N., & Boucher, O. (2023). Sensitivity of cirrus and contrail radiative effect on cloud microphysical and environmental parameters. Atmospheric Chemistry and Physics, 23(21), 14003–14037. https://doi.org/10.5194/acp-23-14003-2023
- Wright, C. J., Osprey, S. M., & Gille, J. C. (2013). Global observations of gravity wave intermittency and its impact on the observed momentum flux morphology. *Journal of Geophysical Research*, 118(19). https://doi.org/10.1002/jgrd.50869
- Yin, F., Grewe, V., Castino, F., Rao, P., Matthes, S., Dahlmann, K., et al. (2023). Predicting the climate impact of aviation for en-route emissions: The algorithmic climate change function submodel ACCF 1.0 of EMAC 2.53. *Geoscientific Model Development*, 16(11), 3313–3334. https://doi.org/10.5194/gmd-16-3313-2023
- Yu, F., Kärcher, B., & Anderson, B. (2024). Revisiting contrail ice formation: Impact of primary soot particle sizes and contribution of volatile particles. Environmental Science and Technology, 58(40), 17650–17660. https://doi.org/10.1021/acs.est.4c04340
- Zhang, C., & Harrington, J. Y. (2014). Including surface kinetic effects in simple models of ice vapor diffusion. *Journal of the Atmospheric Sciences*, 71(1), 372–390. https://doi.org/10.1175/JAS-D-13-0103.1
- Zhang, W., Weverberg, K. V., Morcrette, C. J., Feng, W., Furtado, K., Field, P. R., et al. (2025). Impact of host climate model on contrail cirrus effective radiative forcing estimates. Atmospheric Chemistry and Physics, 25(1), 473–489. https://doi.org/10.5194/acp-25-473-2025

KÄRCHER AND CORCOS 28 of 28